DEVELOPMENT OF PEG-PEPTIDE CONJUGATE BASED CURCUMIN DELIVERY SYSTEMS

A Thesis Submitted to
the Graduate School of Engineering and Sciences of
İzmir Institute of Technology
in Partial Fulfillment of the Requirements for the Degree of

MASTER OF SCIENCE

in Chemical Engineering

by
Gamze AYDOĞAN

December 2022
İZMİR

ACKNOWLEDGEMENTS

I would like to express my gratitude for my advisor Assoc. Prof. Dr. Ayben TOP for her priceless support throughout this study.

I would also like to express my gratitude to my committee members, and Prof. Dr. Muhsin Çiftçioğlu and Assoc. Prof. Dr. Canan Uraz for their suggestions and recommendations.

I would like to thank PhD. Çağdaş TAŞOĞLU for performing MALDI-TOF mass spectroscopy experiments at National Mass Spectrometry Application and Research Center, Filiz KURUCAOVALI who performed HPLC analyses, from Environmental Development Application and Research Center, and Deniz ŞİMŞEK from Department of Chemical Engineering during the characterization studies. I appreciate the help I received from Dr. Hüseyin ÖZGENER for taking NMR data and I am grateful to Yekta GÜNAY and Murat DELMAN from Biotechnology and Bioengineering Application and Research Center for making dynamic light scattering experiments and UV-vis Spectrometry and ATR-FTIR analysis.

Moreover, I was so lucky for the companies always there for me during my studies Selin ŞEN, Burcu SIRMA TARIM, İrem YAKAR and Damla YALÇIN.

Finally, I owe the greatest thanks for the support I received by my family throughout my whole life.

ABSTRACT

DEVELOPMENT OF PEG-PEPTIDE CONJUGATE BASED CURCUMIN DELIVERY SYSTEMS

In this study, a drug delivery system based on Pluronic F127 and a peptide conjugate was proposed. The F127-peptide conjugate was prepared by the reaction between succinimidyl functionalized F127 (SC-F127) and peptide. SC-F127 was synthesized using disuccinimidyl carbonate and DMAP. Folic acid-functionalized F127 (FA-F127) was also prepared to obtain active targeting copolymers. Four peptides containing pH-responsive multiple histidines and endosome disruptive GFWFG domain were synthesized using the Fmoc procedure. H-Gly-2-ClTrt resin and Rink amide MBHA resin were used to synthesize side-chain-protected and deprotected peptides, respectively. 2-chlorotrityl resin failed in synthesizing the high-purity peptides with adjacent histidines in their sequences. Peptide-4 having a sequence of GGH_6GFWFG, was prepared with acceptable purity using rink amide MBHA resin and was conjugated to SC-F127. Curcumin was loaded to F127 and F127-peptide using the thin film method with DCM solvent. Almost all curcumin was encapsulated into F127 micelles. However, the entrapment efficiency % of the F127-peptide micelles was ~86% due to the lower solubility of F127-peptide conjugate in DCM. Dynamic light scattering experiments were used to determine the stability and size distribution of the micelles. Number-based size distributions of both micelles indicated that a single peak between 10 and 30 nm was independent of pH. The peak position did not change upon incubating the micelles at 37ºC up to a few days. Initially, intensity-based results of both samples indicate bidisperse populations at pH 5.0 and 7.4. Curcumin-loaded F127 micelles aggregated in the three days, as revealed by the formation of the third peak above 1000 nm independent of pH. Curcumin-loaded F127-peptide micelles, on the other hand, retain their stability for up to five days at neutral pH. For this sample, the third peak was observed only at pH 5.0 on days 2 and 5.

ÖZET

PEG-PEPTİD KONJUGATI BAZLI KÜRKÜMİN TAŞIYICI SİSTEMLERİNİN GELİŞTİRİLMESİ

Bu çalışmada, Pluronic F127-peptit konjugatı bazlı bir ilaç taşıyıcı sistemi öngörülmüştür. F127-peptit konjugatı, süksinimidil işlevselleştirilmiş F127 (SC-F127) ve peptit arasındaki reaksiyonla hazırlanmıştır. SC-F127, disüksinimidil karbonat ve DMAP kullanılarak sentezlenmiştir. Aktif hedefleme kopolimerleri elde etmek için folik asit işlevli F127 (FA-F127) de hazırlanmıştır. pH'ya duyarlı çoklu histidin ve endozom parçalayıcı GFWFG dizini içeren dört peptit, Fmoc prosedürü kullanılarak sentezlenmiştir. H-Gly-2-ClTrt ve Rink amid MBHA reçineleri sırasıyla yan zincir korumalı ve yan zincir koruması kaldırılmış peptitleri sentezlemek için kullanılmıştır. 2-klorotritil reçinesi, yüksek saflıkta dizinlerinde bitişik histidinler içeren peptitleri, sentezlemede başarısız olmuştur. GGH_6GFWFG dizinine sahip peptid-4, rink amid MBHA reçinesi kullanılarak kabul edilebilir bir saflıkta hazırlanmış ve SC-F127'ye konjuge edilmiştir. Kurkümin, DCM solventi ile ince film yöntemi kullanılarak F127 ve F127-peptide yüklenmiştir. Hemen hemen kurkuminin tamamı, F127 misellerince enkapsüle edilmiştir. Bununla birlikte, DCM'de F127-peptit konjugatının daha düşük çözünürlüğü nedeniyle F127-peptid misellerinin hapsetme verimliliği yüzdesi ~ % 86 olarak elde edilmiştir. Misellerin stabilitesini ve boyut dağılımını belirlemek için dinamik ışık saçılımı deneyleri kullanılmıştır. Her iki miselin sayı bazlı boyut dağılımları, pH'tan bağımsız olarak 10 ila 30 nm arasındaki tek bir tepe noktası göstermiştir. Misellerin 37^{o}C'de birkaç güne kadar inkübe edilmesinden sonra pik pozisyonu değişmemiştir. Başlangıçta, her iki numunenin ışık şiddetine dayalı sonuçları, pH 5.0 ve 7.4'te çift dağılımlı popülasyonları göstermiştir. Kurkumin yüklü F127 miselleri, pH'tan bağımsız olarak 1000 nm'nin üzerinde üçüncü bir pik oluşmasıyla ortaya çıktığı gibi, üç gün içinde kümelenmiştir. Öte yandan, kurkumin yüklü F127-peptit miselleri, nötr pH'ta beş güne kadar stabilitelerini korumuştur. Bu numune için, üçüncü pik 2. ve 5. günlerde ve yalnızca pH 5.0'de gözlenmiştir.

TABLE OF CONTENTS

LIST OF FIGURES

Figure **Page**

Figure **Page**

Figure **Page**

LIST OF TABLES

Table **Page**

ABBREVIATIONS

CMC = Critical micelle concentration

DCM = Dichloromethane

DDS = Drug Delivery System

DIPEA = N,N-Diisopropiletilamin

DEE = Drug entrapment efficiency

DLC = Drug loading capacity

DMF = Dimethyl formamide

DMAP = 4-Dimethylaminopyridine

DMSO = Dimethyl sulfoxide

DOX = Doxorubicin

DSC = N,N' Disuccinimidyl carbonate

EPR = Enhanced permeability and retention

F127 = Pluronic 127

FA = Folic acid

FDA = US Food and Drug Administration

FTIR = Fourier Transform Infrared Spectroscopy

HATU = 1-[Bis(dimethylamino)methylene]-1H-1,2,3-triazolo[4,5-b]pyridinium 3-oxide hexafluorophosphate

HBTU = 2-(1*H*-benzotriazol-1-yl)-1,1,3,3-tetramethyluronium hexafluorophosphate

HCTU = 2-(6-Chloro-1H-benzotriazole-1-yl)-1,1,3,3-tetramethylaminium hexafluorophosphate

HOBt = Hydroxybenzotriazole

HPLC = High Performance Liquid Chromatography

KBr = Potassium bromide

MDR = Multidrug resistance

NMR = Nuclear Magnetic Resonance

PEO = Polyethylene oxide

PPO = Polypropylene oxide

P-gp = P-glycoprotein

TEM = Transmission Electron Microscopy

TFA = Trifluoroacetic acid

ROS = Reactive oxygen species

SC = Succinimidyl carbonate

SPPS = Solid Phase Peptide Synthesis

CHAPTER 1

INTRODUCTION

1.1. Cancer and Treatment Methods

Even though cancer is one of the most invincible diseases with a high mortality rate in modern times, it is not a novel problem for human beings. The oldest definition of cancer with a different name was found in heritage from 3000 BC in Egypt, and it was defined as a disease without any therapy method. Cancer was taken its current name in the Hippocrates period because of its similarity to the shape of a crab (American Cancer Society 2021).

Cancer cells which differ from healthy cells in morphological, molecular, and metabolic aspects, occur at the end of a multi-step process named 'carcinogenesis,' breaking down the working mechanism of the genes that regulate the cell cycle. Carcinogenesis consists of three steps, including initiation, promotion, and progression, as given in Figure 1.1. In the first step of the process, normal cells are affected by chemical, physical, or biological mutagens, and proto-oncogenes become oncogenes. Then, proteins that control the cell cycle cannot be synthesized, and cells start to grow continuously by escaping from the control mechanism. These altered cells form preneoplastic lesions by cell proliferation in the promotion step, as they are resistant to apoptosis and can escape from the immune system. During carcinogenesis, the interaction between endothelial tissue and tumor tissue gets weaker; this makes the easy transition of cancer cells to the blood and lymphatic flow through new veins formed around tumor tissue. Transportation of cancer cells to seconder organs or tissues is named metastases (Burgio ve Migliore 2014).

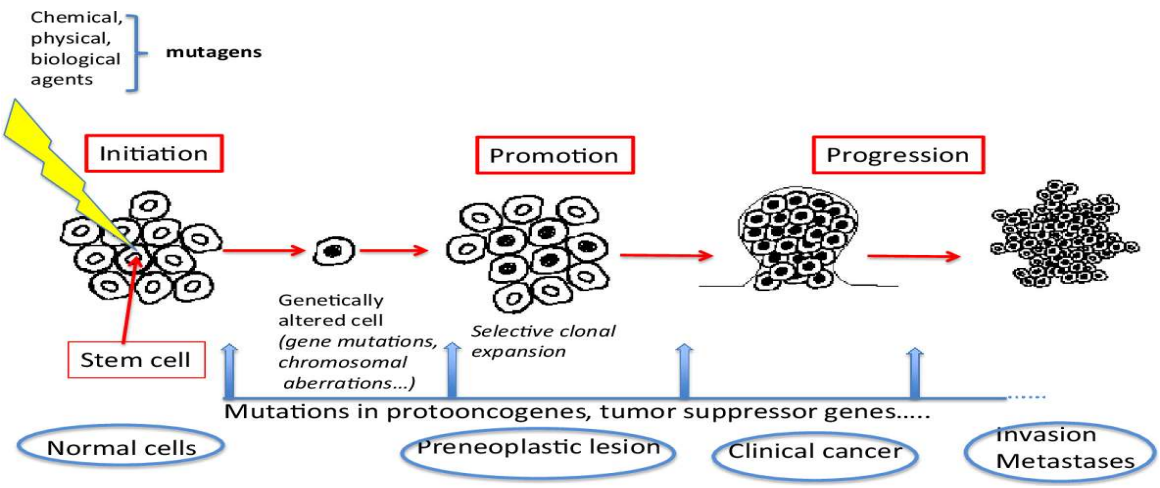

Figure 1.1.Steps of carcinogenesis

(Source: Burgio & Migliore, 2014)

There are three conventional therapy methods for cancer, including radiotherapy, surgery of solid tumors, and chemotherapy.

The utilization of ionizing radiation to kill or stop the growth and division of cancer cells is named radiotherapy. X-rays and gamma-rays can be used for radiotherapy by using an external source, or electrons, neutrons, and protons may be used internally to damage tumor tissues. The application method is chosen according to tumor types, sizes, and localizations. This therapy aims to cure patients by destroying cancer cells by directly damaging their DNA strands and indirectly via generating reactive oxygen species (ROS). (Mortezaee ve Najafi 2020) (Gianfaldoni, et al. 2017).

Many radical and non-radical groups, like hydroxyl radicals, organic radicals, hydrogen peroxides, and singlet oxygens, can be considered ROS. ROS protects cells against mutagenic stimulants and extreme conditions at its basal level in the cell. Nevertheless, as the level of ROS increases in the cell, it cannot continue to protect the cell, and intracellular balance cannot be maintained. ROS becomes harmful to cell membranes, proteins, lipids, and DNA. Then, it starts a series of mutagenic chain reactions and causes changes that cannot be controlled and form cancer cells. So, the formation of DNA strand breaks because of the increasing amount of free radicals in the cell is a disadvantage of radiotherapy (Çiftçi 2017).

Surgery removes solid tumors from the body but is restricted to solid tumors like leukemia, lymphoma, and metastatic cancers. Moreover, surgery causes trauma to the tissues and veins. These damages allow tumor cells to pass into the blood and lymphatic circulation, which may also trigger metastatic cancer development (Tohme, Simmons and Tsung 2017).

Chemotherapy is a drug treatment method developed for 60 years to cure advanced and malignant tumors. The first and second world wars are the major historical occurrences of 20th century that caused millions of people to die, but it was also a breakthrough for cancer treatment. The history of chemotherapy began with artificial dye production by Sir William Henry Perkin. It continued with the discovery of some chemical dyes attached to some tissues selectively by Paul Ehrlich, who won the Nobel Prize in 1908. During the First World War, dye factories started to produce mustard gas. Mustard gas was a cytotoxic gas that caused irreversible harm to people and stopped the ability to produce blood cells. In 1943, the first chemotherapy nitrogen mustard was used on cancer patients successfully, and the development of chemotherapy continued with the discovery of the helical structure of DNA. After that, different concepts, modeling, and drug combinations were developed for various cancer types (Ledford 2020) (Encyclopedia Brittanica 2021) (The Nobel Prize 2021) (Galmarini, Galmarini ve Galmarini 2012).

Despite the high killing rate of cancer cells, chemotherapy has many disadvantages. It disrupts DNA synthesis and cell division and causes side effects like damaging healthy cells, tiredness, hair loss, vomiting, and weight loss. In order to overcome these drawbacks, targeted drug delivery systems can be used.

1.2. Targeted Drug Delivery

There are numerous natural chemotherapeutic agents and FDA-approved synthetic drugs to kill cancer cells. The main challenge of chemotherapy is adjusting drug dosage that maximizes efficacy and minimizes treatment toxicity. So, the main idea of targeted drug delivery systems is to reach maximum toxicity on cancer cells using the minimum amount of chemotherapeutics by minimizing adverse effects on patients (Laffleur and Keckeis 2020).

Many chemotherapeutics are hydrophobic, resulting in insufficient solubilization in physiological fluids and low bioavailability. Drug delivery systems can improve insoluble drugs' bioavailability by prolonging blood circulation time. Thus, they improve the effectiveness of chemotherapeutics at tumor sites and protect healthy cells from the toxic effects of drugs. They can also increase cytotoxicity via fast and triggered release at the tumor site. Polymer-based nanocarriers (polymeric nanoparticles, polymeric micelles, polymer-drug conjugates), liposomes, and inorganic nanoparticles (such as carbon nanotubes, gold and silica nanoparticles) have been used for drug delivery systems (Laffleur and Keckeis 2020) (Vasir and Labhasetwar 2005) (Baran 2018).

Drug delivery systems can be transported to the tumor tissues passively or actively. Passive targeting is the transportation of drugs to tumor sites by exploiting enhanced permeability and retention (EPR). Figure 1.2 presents the basic principle of the EPR effect. Pores in normal endothelial cells are smaller than 2 nm, but their width in tumor tissues increases up to 500 nm as the vascular endothelial growth factor is stimulated. The EPR effect allows the accumulation of drugs in tumor tissues passively (Baran 2018).

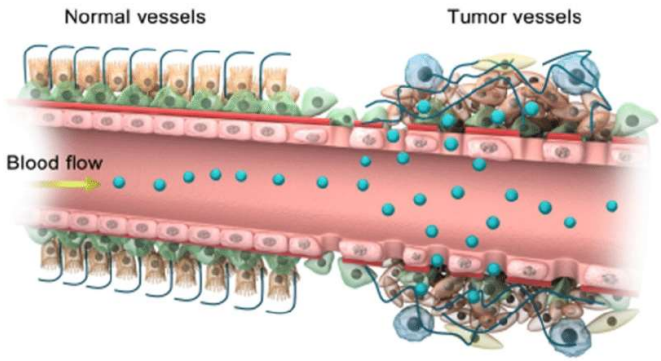

Figure 1.2. Passive Targeting of Chemotherapeutics via EPR effect

(Source: Abdalla, et al., 2018)

Active targeting, also known as ligand-based targeting, exploits the overexpression of receptors on the surfaces of cancer cells (Figure 1.3). Due to the high metabolic rate of cancer cells, the number of receptors on the cell surface increases. Thus, drug delivery systems can be designed with ligands binding specifically to these receptors. Transporting systems can be modified with peptides (RGD peptide sequence), vitamins (folic acid), sugars (mannose and galactose), and antibodies (anti-Her2, anti-CD24). Active targeting increases drug accumulation and toxicity in tumor tissues and eliminates the side effects of chemotherapeutics on healthy cells (Baran 2018).

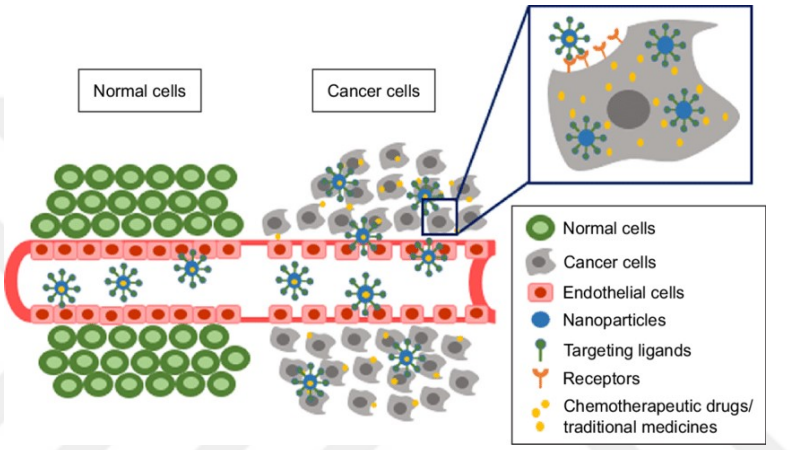

Figure 1.3. Active targeting of Drug Delivery Systems

(Source: Muhamad, Plengsuriyakarn, & Na-Bangchang, 2018)

Folic acid, also known as vitamin B9, is one of the B vitamins found in green leaves, mushrooms, beans, and peanuts. Folic acid can be used as an active targeting ligand as it binds to the overexpressed folate receptors (especially FRα) on cancer cells. Folic acid consists of three main parts pterin, ρ-amino-benzoate, and glutamate (Figure 1.4). Folic acid can be used as an active targeting ligand via its pterin part, and glutamate moiety of folate receptors on the cell surface bind each other (Harvard T.H. Chan School of public health 2021) (Chen, et al. 2013).

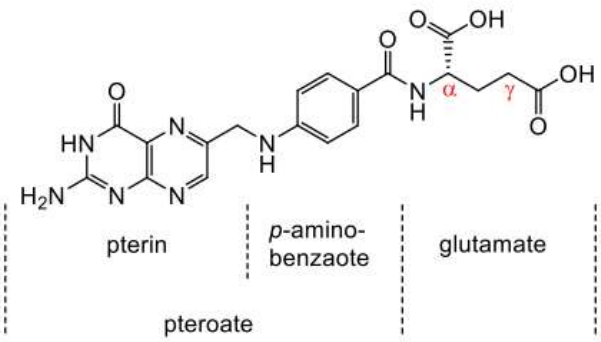

Figure 1.4. Molecular structure of folic acid

(Source: Boss & Ametamey , 2020)

Stimuli-responsive drug delivery systems can be activated after accumulation in cancer cells by specific inner or outer body triggers. Stimuli-responsive systems can be used to increase blood circulation time, improve the effectiveness of chemotherapeutics by improving drug release in the tumor sites and decrease side effects on healthy cells, and also be used to hinder drug leakage during transport. These systems are divided into two groups internal stimuli and external stimuli systems. External stimuli systems can be electromagnetic, light, radiation, or ultrasound responsive. Cancer cells have different environments than normal ones, like having lower pH and higher temperature because of their abnormal activity. Thus, pH, temperature, and redox potential can be exploited as internal stimulants. Internal-stimuli responsive systems are more efficient than the others as the stimulants already exist in sites where the drug is applied (Liu, et al. 2017) (Yao, Feng and Chen 2016).

1.3. Curcumin

Turmeric (Curcuma longa) is one of the most indispensable species, especially in Asian cuisine, which can also be used in different areas like medicine, wound healing, dye, and cosmetics. Curcumin is a yellow, polyphenolic, main active turmeric compound isolated from its rhizomes. Curcumin has antioxidant, anti-inflammatory, antiviral, antibacterial, antidiabetic, and anticancer properties attributed to different functional groups, as outlined in Figure 1.5. The anticancer effect of curcumin is due to

the presence of OH groups in its structure. Despite having great benefits against many diseases, the applications of curcumin are limited due to its low solubility and low oral bioavailability. The reasons for its poor bioavailability are its poor absorption, high metabolism rate, and excretion, rapid clearance and elimination rate from the body, especially when it is administered orally (Jankun , et al. 2016) (Hewlings and Kalman 2017) (Zhang, et al. 2013) .

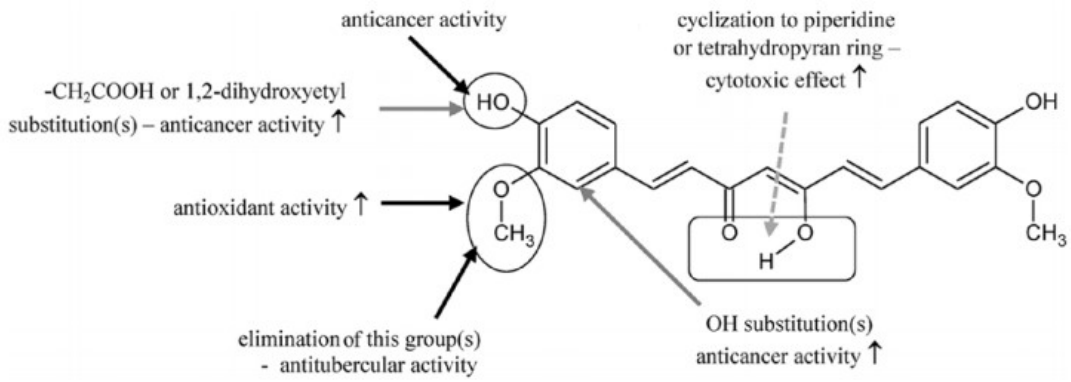

Figure 1.5. Structure-activity relationships of curcumin derivatives

(Source: Jankun, et al., 2016)

Curcumin is absorbed mainly in the basic environment after the stomach when it is administered orally. Two phenolic protons and one enolic proton with respective pKa values of 10-10.5 and 8.5 ensure the absorption of curcumin at basic conditions. However, curcumin cannot dissolve in neutral and acidic conditions. It is absorbed thoroughly in the intestines after hydrolyzation. Then, it is removed from the body resulting in a low blood concentration of curcumin and, hence, its low bioavailability. Polymeric micelles, liposomes, and various nanoparticles and microemulsions have been developed to cope with curcumin's low solubility and bioavailability (Hewlings and Kalman 2017) (Ma, et al. 2019).

Curcumin is proposed to be an effective chemotherapeutic agent in the treatment of various cancers, including breast, colorectal and gastrointestinal cancers. It affects

various cell pathways like apoptosis, cell proliferation, angiogenesis, and cell cycle. At the molecular level, curcumin can inhibit cell metastasis and induce cell apoptosis by regulating pro-inflammatory cell factors and epidermal growth factor receptors, growth factors such as epidermal growth factor, transcription factors, apoptosis-related enzymes, and proteins. (Ma, et al. 2019).

Multidrug resistance (MDR) is a significant obstacle that limits chemotherapeutics' efficacy in tumor cells. MDR is attributed to the overexpression of the efflux proteins such as P-glycoprotein (P-gp), mitoxantrone resistance protein (ABCG2), and multidrug resistance-associated protein 1 (MRP-1) in the cell membrane. After the chemotherapeutics are administrated to the cells, these proteins are stimulated. Then, the intracellular drug concentration is decreased by transporting the drug out of the cell. Overexpression of P-gp, an ATP-dependent membrane transporter, decreases the drug concentration in the nucleus and even the cytoplasm of tumor cells, increases the elimination of drugs and decreases penetration of drugs to tissues acting as a drug efflux system. Hence, cancer cells become more resistant to therapeutics. Despite exposure to anticancer drugs, these cells can survive by exploiting MDR. Curcumin can reverse drug resistance of cancer cells by inhibiting the expression and function of these three MDR-associated proteins in the tumor cell (Ma, et al. 2019) (Rodrigues, et al. 2017).

Various tumor suppressor genes like p53, APC, and WT1 regulate the cell cycle to prevent tumor formation in the body and control apoptosis (programmed cell death). These genes can control cell growth, restrain the abnormal growth of the cell, and prevent tumor formation by inducing apoptosis. Mutation in these genes causes inhibition of cell apoptosis, formation, and development of tumor cells and chemotherapeutic resistance. p53 is considered the major tumor suppressor gene because the mutant p53 gene is seen in almost 50% of human cancer types like breast, brain, and lung cancers. Mutations in p53 cause the lack of apoptosis control and the abnormal growth of the cell and, hence, tumor formation. Curcumin prevents abnormal growth of cancer cells and ensures apoptosis by stabilizing the p53 gene (Harris 1996) (Patiño-Morales , et al. 2020).

1.4. Poloxamers

Liposomes, polymeric micelles, polymer-drug conjugates, inorganic nanoparticles, and nanocrystals have been employed as drug delivery systems. Polymeric micelles in which the drug is physically entrapped (Figure 1.6) can easily be prepared compared to the polymer-drug conjugates. The nanoparticles smaller than 5.5 nm cannot escape from the renal system and are removed from the body. On the other hand, nanoparticles larger than 200 nm accumulate in the liver and spleen. Therefore, the nanoparticles with sizes between 10 and 100 nm offer prolonged circulation time in the vascular system and accumulate at the tumor site selectively by exploiting the EPR effect (Baran 2018) (Rapoport 1999).

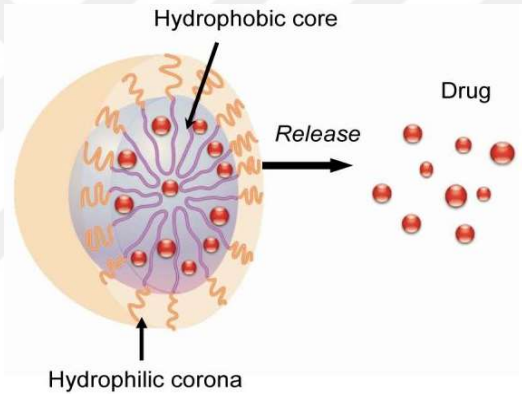

Figure 1.6. Micellar Drug Delivery System

(Source: Batrakova & Kabanov, April 2008)

Poloxamers are amphiphilic three-block copolymers consisting of hydrophilic polyethylene oxide (PEO) and hydrophobic polypropylene oxide (PPO) chains bonded covalently. They are also known as 'Pluronic.' Above the critical micelle concentration (CMC), Pluronic micelles composed of a hydrophobic core and a hydrophilic corona are formed in aqueous solutions. Their chemical and physical properties, CMC values, and in vivo properties and interactions with cells and cell membranes can be tuned with the ratio between chain lengths of PPO and PEO blocks as given in Table 1.1 (Pitto-Barry and Barry 2014). Poloxamers can encapsulate drugs in their hydrophobic core, increase the solubility and blood circulation time of the drugs, and enhance drug transport across

cellular barriers. Pluronic micelles have high potential as drug delivery systems due to their biocompatibility and high drug encapsulation capacity, and appropriate sizes for the EPR effect (Baran 2018) (Pitto-Barry and Barry 2014) (Batrakova and Kabanov 2008).

Table 1.1. Representative molecular structure and properties of Pluronic block copolymers

(Source: Pitto-Barry & Barry, 2014)

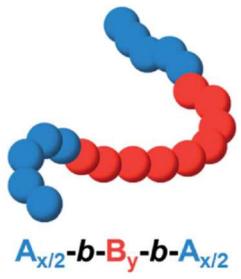

Pluronic®	Average no. of EO units (x)	Average no. of PO units (y)	Molar Mass	Cloud point in 1% aqueous solution (°C)	HLB	CMC (M)
L61	4.55	31.03	2000	24	3	1.1×10^{-4}
L121	10.00	68.28	4400	14	1	1.0×10^{-6}
F127	200.45	65.17	12600	> 100	22	2.8×10^{-6}
F68	152.73	28.97	8400	> 100	29	4.8×10^{-4}
F87	122.50	39.83	7700	> 100	24	9.1×10^{-5}
P105	73.86	56.03	6500	91	15	6.2×10^{-6}
P123	39.20	69.40	5750	90	8	4.4×10^{-6}

HLB = hydrophilic–lipophilic balance; CMC = critical micelle concentration; Data from reference 24

Additionally, Pluronic polymers can adjust the viscosity of cell membranes and increase drug concentration in cancer cells by inhibiting of activities of P-gp proteins. Thus, they can reverse the MDR and increase the apoptosis of cancer cells as given in Figure 1.7 (Batrakova and Kabanov 2008) (Hong, et al. 2017).

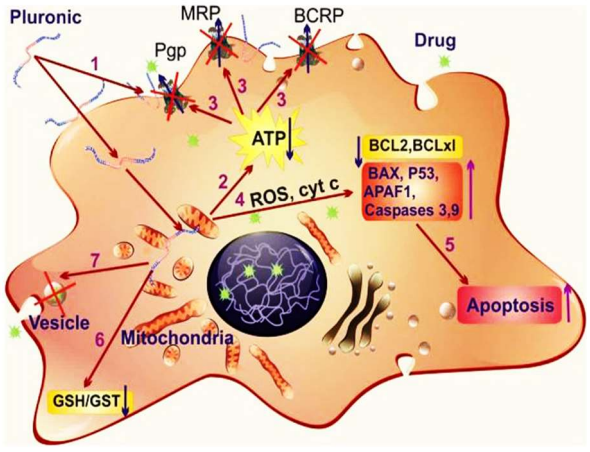

Figure 1.7. Effect of Pluronic on biological processes cancer cells

(Source: Batrakova & Kabanov, April 2008)

1.5. Endosomal Escape Mechanism

Macromolecule describes the molecules with molecular weights higher than 1,000 Da. The size of these molecules, such as polymers, nucleic acids, and proteins, usually ranges between 10^{-5} to 10^{-3} mm (100 to 10,000 angstroms) (Britannica 2022). Macromolecules are internalized by cells via endocytosis, different from small molecules. There are three types of endocytosis phagocytosis, pinocytosis, and receptor-mediated endocytosis. Endocytosis is observed only in cells without a cell wall. The mechanism of the endocytosis of macromolecules is given in Figure 1.8. Firstly, the macromolecule is recognized by the cell and wrapped entirely by the cellular membrane in all of these mechanisms. These molecules are taken into the cell by a small vesicle named the early endosome at a pH of 6.3. Then, the late endosome is formed from the early vesicle with the acidification in time, and the pH value reaches almost 5.5 inside the endosome. At the end of the endocytosis process, the late endosome is digested with lysosomal enzymes (Pei ve Buyanova 2018) (Cooper 2000).

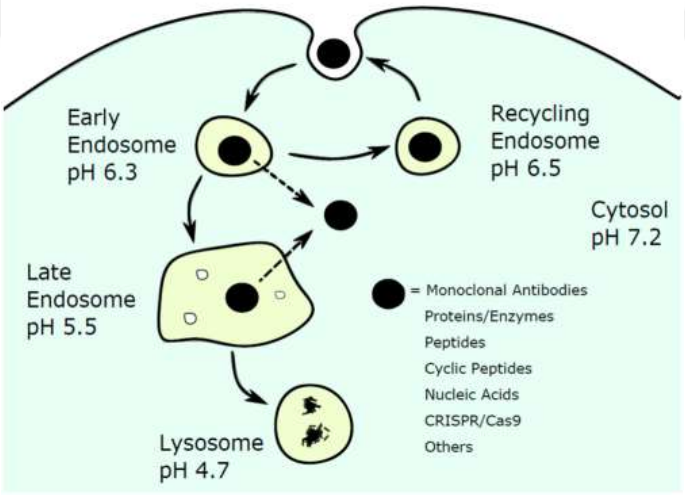

Figure 1.8. Endocytosis of macromolecules

(Source: Pei & Buyanova, 2018)

Before being degraded by hydrolytic enzymes, drug delivery systems with chemotherapeutic agents must escape from inside the endosome. Macromolecules can escape from endosomal fusion by proton sponge effects osmotic lysis, pore formation,

membrane destabilization, or membrane fusion (Pei ve Buyanova 2018). Amino acids with aromatic side chain groups can destabilize the cell membrane by embedding their aromatic side chains into the lipid bilayer. This interaction causes local membrane destabilization and transportation through the membrane (Lönn, et al. 2016) (Pei ve Buyanova 2018).

This study aims to prepare an anticancer drug delivery system by conjugating Pluronic F127 with the peptide containing pH-sensitive polyhistidine part and an endosome disruptive unit. Curcumin was encapsulated into the hydrophobic core of peptide-copolymer conjugate to increase the solubility and bioavailability of curcumin. The following literature review chapter (Chapter 2) presents examples of various drug carrier systems (Pluronic micellar systems, responsive and targeted DDSs), In Chapter 3, materials and synthesis procedures used in the preparation of the drug delivery system are detailed, and characterization techniques are described. In Chapter 4, characterization results of the peptides, the F127-peptide system, and curcumin-loaded DDSs (F127 and F127-peptide conjugate) are given. Chapter 5 concludes this thesis with the most striking results of this study and future experimental plans.

CHAPTER 2

LITERATURE REVIEW

In this chapter, applications of Pluronic micelle-based drug delivery systems for cancer therapy were reviewed. Examples of drug delivery systems with pH-responsive, active targeting, and endosome-disruptive units were outlined.

2.1. Pluronic Micelles in Cancer Therapy Applications

FDA-approved Pluronics with various hydrophilic and hydrophobic block compositions have been investigated as potential carrier systems for anticancer drugs. In one of these studies, curcumin was encapsulated in Pluronic P127 and F68 micelles. Curcumin encapsulation was performed by the thin film hydration method. The effect of the Pluronic type and drug-to-copolymer ratio on drug loading and drug entrapment efficiency were investigated. The results are given in Table 2.1. Compared to Pluronic F68, Pluronic F127 exhibited higher curcumin encapsulation efficiency, which can be attributed to the longer PPO block and higher molecular mass of the F127. Additionally, as the drug-to-polymer ratio increases, curcumin encapsulation efficiency increases for both the Pluronic copolymers. On the other hand, maximum drug loading was obtained at a particular drug-to-polymer ratio for each copolymer.

AFM images of the micelles showed that they are spherical and have sizes between 20 and 80 nm. Curcumin release kinetic profiles of the F127, and F68 micelles are presented in Figure 2.1. F127 released curcumin with a slower kinetic. Half of the incorporated curcumin required 36 h and 144 h for the F68 and F127, respectively. Finally, free curcumin and the curcumin-loaded Pluronic micelles showed similar cytotoxicity against HeLa cells (Sahu, et al. 2011).

Table 2.1. Percentages of drug encapsulation and loading at different ratios of F68 and F127

(Source: Sahu, Kasoju, Goswami, & Bora, 2011)

Pluronic type	Drug:Pluronic ratio (w/w)	Drug encapsulation (%)	Drug loading (%) (w/w)	Drug loading (%) (M/M)
Pluronic F68	1:5	25.72±1.19	4.29±0.19	21.08±0.98
	1:10	34.53±0.74	3.14±0.07	23.98±0.52
	1:25	55.01±0.81	2.12±0.05	26.23±0.57
	1:50	70.24±1.34	1.38±0.04	21.99±0.69
Pluronic F127	1:5	34.33±1.24	5.72±0.21	29.94±1.07
	1:10	46.20±1.40	4.20±0.13	37.74±1.08
	1:25	79.05±1.52	3.04±0.06	45.66±0.88
	1:50	95.57±1.65	1.87±0.03	38.81±0.67

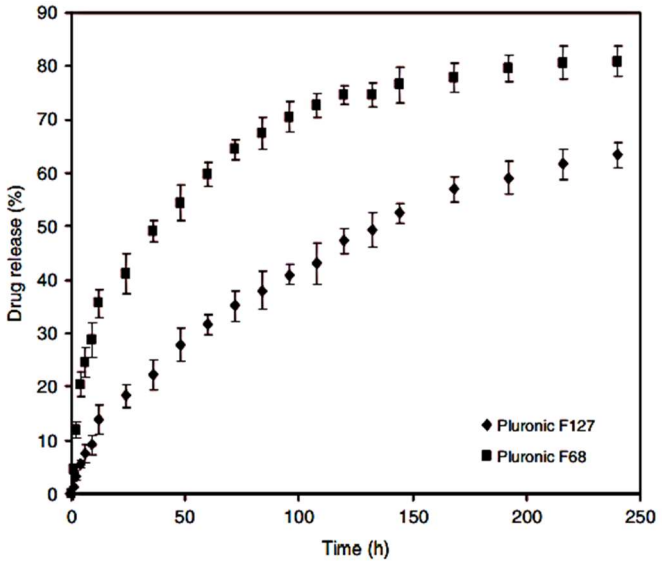

Figure 2.1. In vitro drug release profile of F127 and F68 at pH 7.4 and 37°C

(Source: Sahu, Kasoju, Goswami, & Bora, 2011)

In another study, curcumin was encapsulated into mixed micelles containing P123 and F68 Pluronic copolymers. Curcumin loading and encapsulation efficiency

percentages were determined by changing the initial amount of curcumin and the ratio between P123 and F68 copolymers. The optimum amount of curcumin and the ratio between P123 and F68 copolymers are found as 17.3 mg 2.05, respectively. Moreover, at these optimal conditions, the solubility of the encapsulated curcumin in micelles was obtained 27,500 times higher compared to that of the curcumin in aqueous solutions.

Encapsulation of curcumin into mixed micelles also slows the curcumin release kinetics (Figure 2.2). In the first ten hours, 15% of the encapsulated drug was released from micelles, whereas the release of the free curcumin from the propylene glycol solution was almost 70%. Thus, curcumin release from Pluronic micelles ensures a sustainable release profile and minimizes burst release of the curcumin. Cytotoxicity of free curcumin, empty, and curcumin-loaded micelles was determined by MTT assay. Curcumin-loaded mixed micelles exhibited the highest toxicity against MCF-7 and adriamycin-resistant MCF-7 (MCF-7/ADR) cells, indicating the potential of Pluronics in the reversal of MDR (Zhao, et al. 2012).

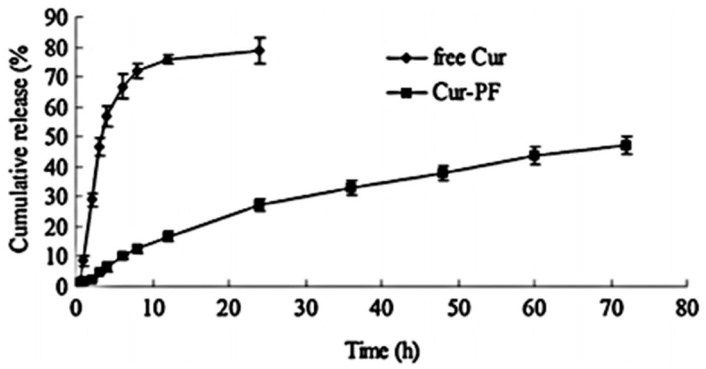

Figure 2.2. Cumulative release of curcumin from mixed micelles and curcumin solution with the propylene glycol

(Source: Zhao, et al., 2012)

2.2. pH responsive Drug Delivery Systems

pH-responsive drug delivery systems can be prepared by incorporating ionizable functional groups into the system or using a pH-sensitive chemical bond between the DDS and the drug. In one of the recent studies, pH-responsive self-assembling cationic peptide I_6K_5 was investigated for doxorubicin (DOX) delivery. Hydrodynamic diameters of self-assembled cationic peptides were measured using dynamic light scattering (DLS) in the neutral and acidic environment and are given in Figure 2.3a. At pH 7.4, only one peak was observed at approximately 100 nm, whereas at pH 6, the intensity of this peak decreased, and another peak was observed at 295 nm. Similarly, Figure 2.3b indicates cumulative drug release at the acidic pH was higher than that at the neutral condition, confirming the pH responsiveness of the I_6K_5 peptide (Gong, et al. 2020).

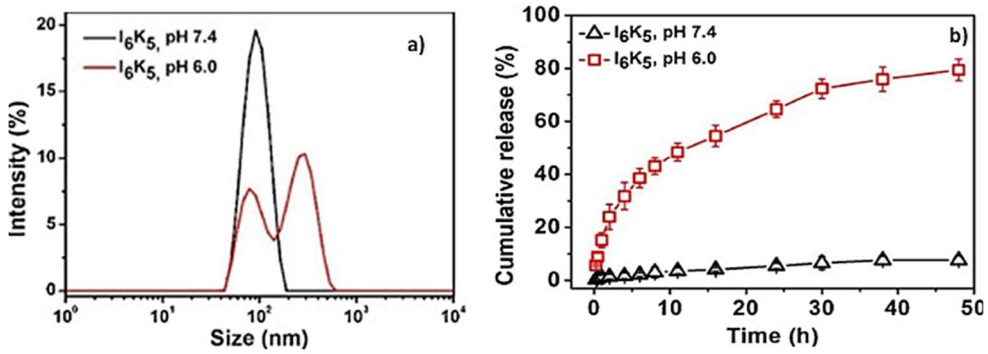

Figure 2.3. a) Hydrodynamic sizes of I6K5 peptide and b) Cumulative drug release from I6K5 peptide at pH 7.4 and 6.0

(Source: Gong, et al., 2020)

MTT assay was used to test the cytotoxicity of I_6K_5 on the human liver cell line (L02) and the human hepatocellular carcinoma cell line (Bel-7402). The results are given in Figure 2.4.a. and Figure 2.4.b. At low concentrations, I_6K_5 is not cytotoxic to both cell lines. Cell viability declined at the peptide concentrations higher than 125 μM. Moreover, the drug-loaded cationic peptide decreased the survival rate of the cells compared to the bare drug (Gong, et al. 2020)

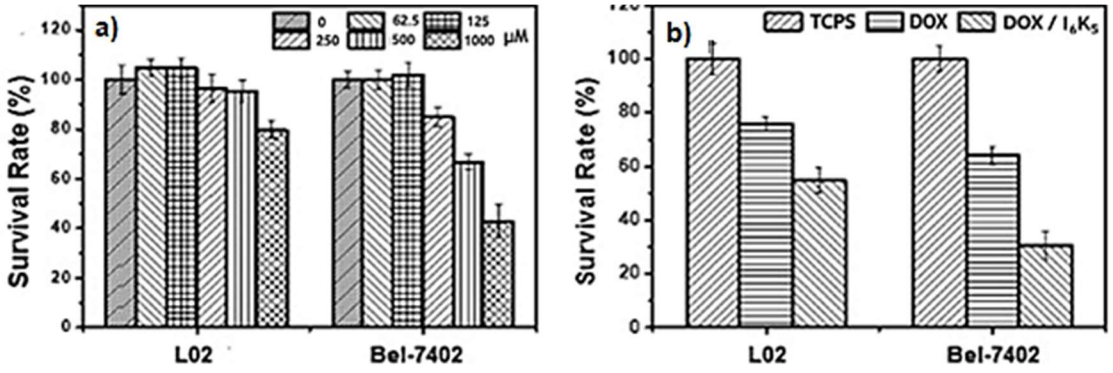

Figure 2.4. Cytotoxicity of a) different concentrations of I6K5 peptide and b) DOX and DOX encapsulated I6K5 nanoparticles on L02 cells or Bel-7402 cells at the end of 24h

(Source: Gong et al., 2020)

In another study, a pH-responsive LHHLLHHLHHLLHH-NH2 (LH) peptide derived from a cell-penetrating peptide with a sequence of LKKLLKLLKKLLKL-NH2 (LK) was used to conjugate camptothecin (CPT). Lysines were replaced with histidines to obtain a pH-sensitive and less toxic peptide. Cytotoxicity of the LK and LH peptide sequences against HeLa and MDA-MB-231 cells was determined using the MTT assay. Figure 2.5.a. and Figure 2.5.b. compare to the LH peptide, the LK peptide is more cytotoxic even at low concentrations. Lactate dehydrogenase (LDH) leakage assay indicates that the LH peptide has membrane transduction activity only at pH 6.0. In contrast, the LK peptide can penetrate cells at pH 6.0 and 7.4 (Zhang , et al. 2019).

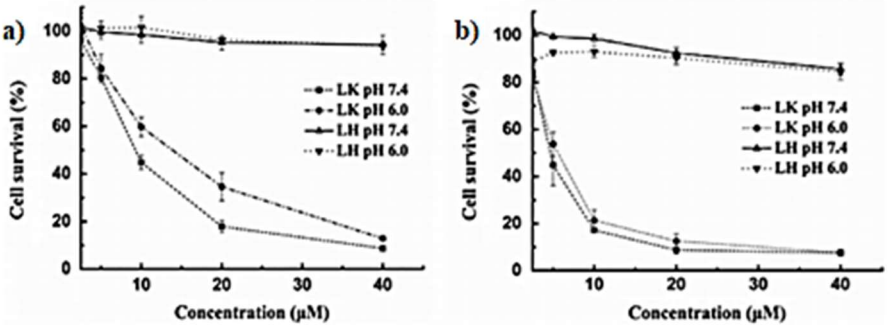

Figure 2.5. Cytotoxicity of LK and LH peptides against a) HeLa cells and b) MDA-MB-231 cells at pH 7.4 and 6.0

(Source: Zhang , et al., 2019)

Fang et al. 2016, prepared a pH-responsive drug delivery system in which curcumin was conjugated with copolymer via a pH-responsive cis-aconitic anhydride linker. pH sensitivity of the DDS was confirmed by monitoring the time course change in the average sizes of micelles at pH 5.0 and pH 7.4 (Figure 2.6). The average size of the DDS is about 100-150 nm at pH 7.4 and did not change significantly during 24 h. At acidic pH, the average size of the micelles initially measured as ~120 nm increased to ~1000 nm after 24 h. MTT assay was applied to compare the cytotoxicity of free curcumin and the F68-curcumin conjugate. At low concentrations, similar cell viability was observed for both free and conjugated curcumin. As the concentration increases, the cell-killing ability of conjugated drug becomes higher than that of free curcumin. As a result, the IC50 value of the curcumin-Pluronic conjugate was obtained as half of that of free curcumin (Fang, et al. 2016).

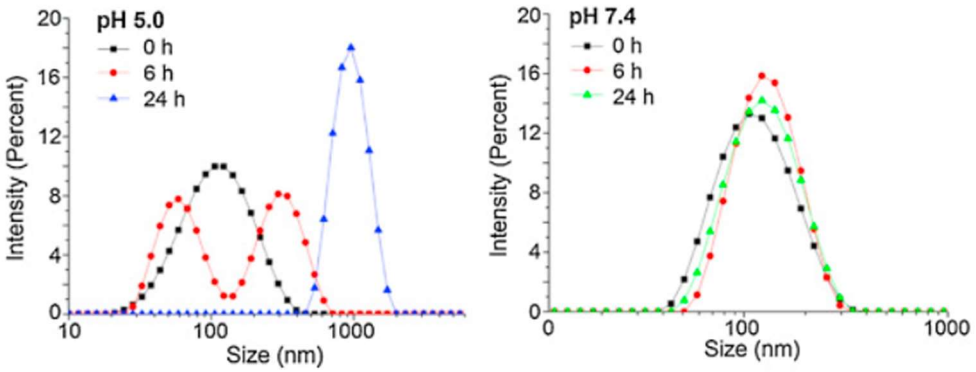

Figure 2.6. Average hydrodynamic sizes of the Pluronic-curcumin micelles at pH 5.0 and 7.4

(Source: Fang, et al., 2016)

2.3 Active Targeting Drug Delivery Systems

In most studies, active targeting was provided by attaching folic acid (FA) to the DDS. Folic acid binds to overexpressed folate receptors on the cancer cells. Jifu et al. (2017) prepared an active targeting micellar drug delivery system by mixing folate-Pluronic conjugate with D-α-tocopheryl polyethylene glycol 1000 succinate (TPGS). A model anticancer drug resveratrol was loaded to the DDS by thin film method. The

mean size of micelles was measured as 20 nm. Cell uptake and cytotoxicity experiments were performed using folate receptor overexpressing MCF-7 cell line. Fluorescence images of internalized micelles without FA (P127) and with FA (P127-FA) are given in Figure 2.7, indicating higher cell uptake efficiency of P127-FA micelles. Thus, folate-containing micelles have both active and passive targeting abilities.

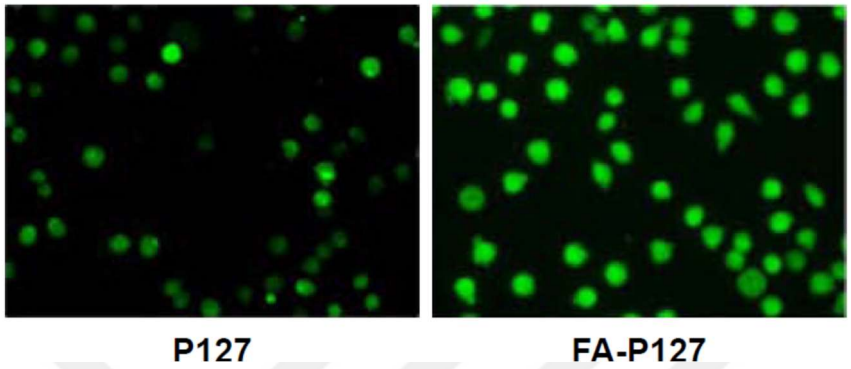

Figure 2.7.Cellular uptake results of P127 and FA-P127

(Source: Jifu, et al., 2017)

Cytotoxicity results of the samples are given in Figure 2.8. Blank P127 and P127-FA micelles exhibit low toxicity up to 50 µg/ml concentration. The highest toxicity was observed for the drug-loaded P127-FA micelles (Jifu, et al. 2017).

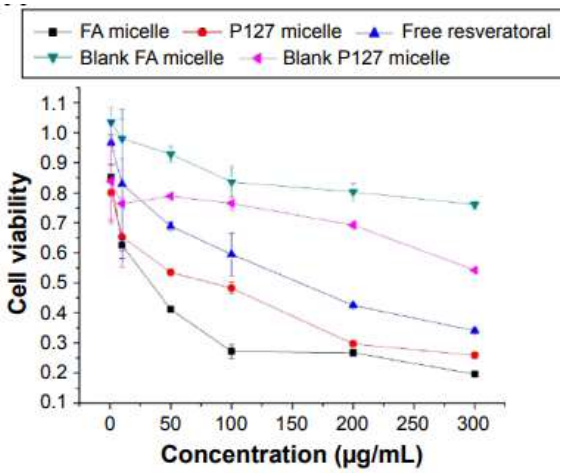

Figure 2.8. Cytotoxicity of free resveratoral and drug loaded micelles on MCF-7 cells

(Source: Jifu, et al., 2017)

The performance of the DDSs can also be improved by combining pH-sensitive and active targeting features. An example of this kind of system was prepared by Ghalehkhondabi et al. (2021). They used anionic poly(methacrylic acid) (PMAA) having carboxylic acid groups with a pKa value of 5.5. These functional groups are protonated at acidic conditions but become negatively charged at pH above 5.5. Folic acid was conjugated to the hydroxyl groups of PMMA, and DOX was used as a model anticancer drug. The DOX release profile of the FA-conjugated PMMA micelles (FA-PMMA) was obtained at pH 5.5 and 7.4 and is shown in Figure 2.9. Increased DOX release at pH 5.5 demonstrates the pH-responsive behavior of the DDS. Figure 2.10 indicates the cytotoxicity results of free DOX and the micellar systems. Empty FA-PMMA micelles are not toxic up to 200 μg/ml concentration. Drug-loaded PMAA-FA showed the highest cytotoxicity against MCF-7 cells, which can be attributed to the active targeting moieties of the DDS (Ghalehkhondabi, Fazlali and Soleymani 2021).

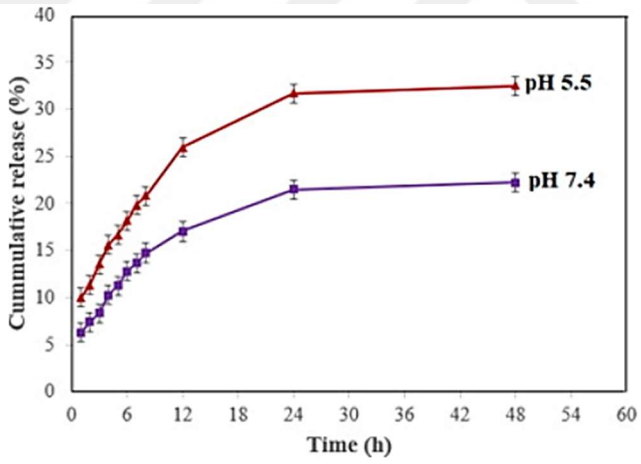

Figure 2.9. DOX release profile of FA-PMAA at pH 5.5 and 7.4

(Source: Ghalehkhondabi, Fazlali, & Soleymani, 2021)

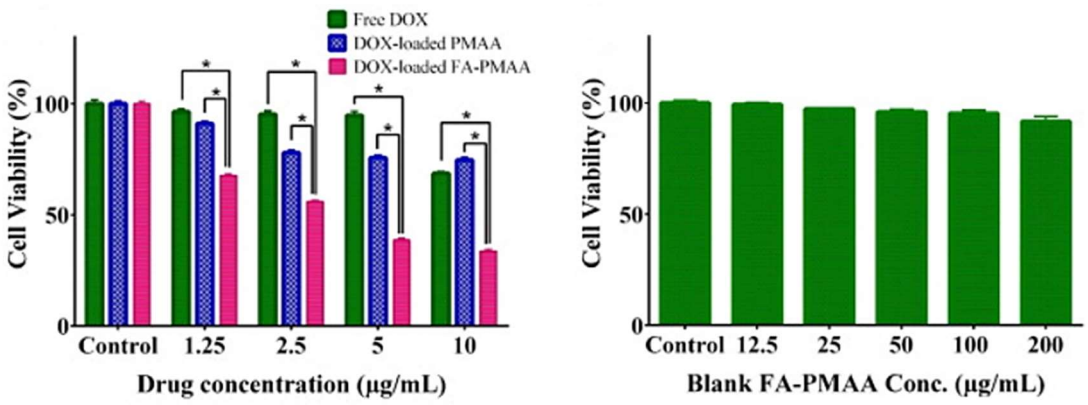

Figure 2.10.Cytotoxicity results of free Dox, Dox-loaded PMAA, Dox-loaded FA-PMAA and Blank FA-PMAA

(Source: Ghalehkhondabi, Fazlali, & Soleymani, 2021)

2.4. Cell Penetrating and Membrane Disruptive Units used Drug Delivery Systems

TAT peptide with positively-charged amino acids, arginine, and lysine is widely used to amplify the internalization of the DDSs. In one of these studies, doxorubicin was conjugated to the cell-penetrating TAT peptide (CGGGYGRKKRRQRRR) to reverse the multidrug resistance of cancer cells. The efficacy of the drug-conjugated cell-penetrating peptide was assessed using drug-resistant and drug-sensitive cells. Figure 2.11 and 2.12 indicate the survival % of respective sensitive and resistant MCF-7 cells exposed to free DOX and DOX-TAT peptide conjugate. Both free drug and DOX-TAT peptide conjugate presented similar cytotoxicity against the sensitive cells. However, the DOX-TAT peptide was observed to be more cytotoxic to drug-resistant MCF-7 cells compared to free DOX. This result can be attributed to the inhibition of drug efflux transporters by TAT-peptide, which leads to high drug concentrations inside the resistant cancer cells. The P-gp inhibition ability of the TAT peptide was verified using a P-gp inhibitor, Verapamil, in the cytotoxicity experiments. The addition of Verapamil decreased the IC50 value of free doxorubicin from 45.2 µM to 6.7 µM

whereas the IC50 value of drug-conjugated TAT peptide did not change in the presence of Verapamil (Liang and Yang 2005).

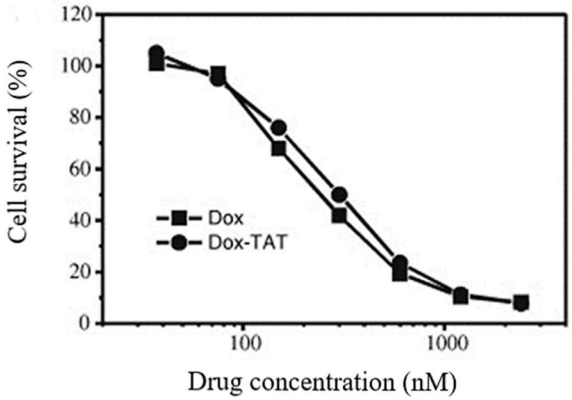

Figure 2.11. Cytotoxicity of free doxorubicin and drug conjugated TAT peptide against drug sensitive MCF-7 cells

(Source: Liang & Yang, 2005)

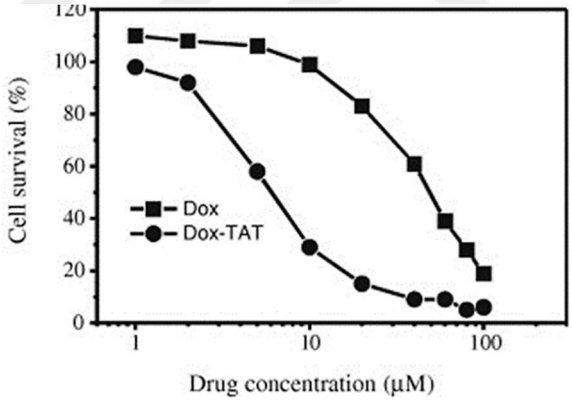

Figure 2.12. Cytotoxicity of of free doxorubicin and drug conjugated TAT peptide on drug resistant MCF-7 cells

(Source: Liang & Yang, 2005)

Lönn et al. (2016) designed several peptide sequences containing aromatic side chains as endosome disruptive domains (EED). These peptides were designed to have tryptophan and phenylalanine in their sequences, as the aromatic side chains can destabilize cell membranes. A green fluorescence protein (GFP) complementation fluorescence assay was used to monitor the endosomal escape property of the candidate

sequences. In this assay, the hydrophobic peptides were conjugated to the TAT-GFPβ11 peptide. A fluorescence signal was obtained upon complexation of the GFPβ11 peptide with the non-fluorescent GFPβ 1-10 protein fragment in the cytoplasm, as given in Figure 2.13. Of the sequences investigated, GFWFG exhibited the highest endosome disruption ability with acceptable cytotoxicity (Lönn, et al. 2016).

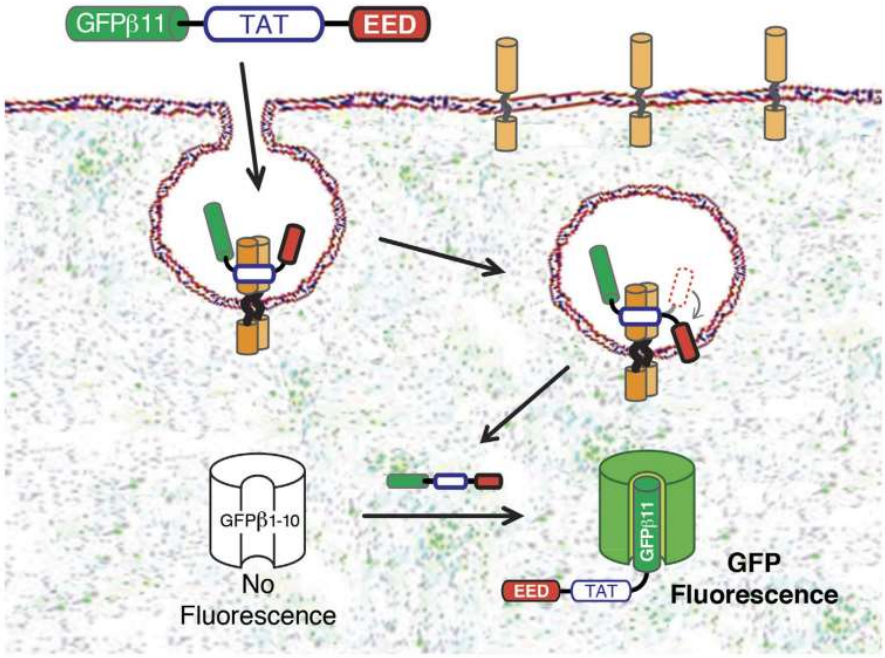

Figure 2.13.Green fluorescence protein (GFP) complementation fluorescence assay used to screen endosome disruptive domains

(Source: Lönn, et al., 2016)

CHAPTER 3

MATERIALS AND METHODS

3.1. Materials

For solid phase peptide synthesis, Glycine-2-Chlorotrityl (H-Gly-2-ClTrt) resin (NovaBioChem), rink amide MBHA resin (NovaBioChem), Fmoc-Gly-OH (NovaBioChem), Fmoc-His(Trt)-OH (NovaBioChem), Fmoc-Ser(tBu)-OH (Aldrich), Fmoc-Phe-OH (NovaBioChem), Fmoc-Trp(Boc)-OH (Aapptec), Fmoc-Gln(OtBu)-OH (NovaBioChem), HOBt (P3 Biosytems), HATU (Carbosynth), HCTU (Carl Roth), DMF (Sigma-Aldrich), DMSO (Isolab), DIPEA (Carl Roth) and piperidine (Acros) were used. Peptide cleavage and deprotection reactions were performed using synthesis grade trifluoroacetic acid (TFA, Carlo Erba), anisole, thioanisole (Sigma), 1,2-ethanedithiol (EDT, Fluka), diethyl ether (DEE, Sigma) and dichloromethane (DCM, Sigma).

For the functionalization reactions, Pluronic F127, DMAP, and regenerated cellulose dialysis membrane (MWCO 14 kDa) were purchased from Sigma-Aldrich. Additionally, N, N'-disuccinimidyl carbonate (Carl Roth), folic acid (Merck), and HBTU (Aapptec) were employed. Anhydrous solvents, acetone, and 1-4-dioxane were provided by Acros Organics. HisPur Ni-NTA resin (Thermo Scientific) was used to separate the unconjugated polymer from the peptide-polymer conjugate.

In the preparation of the buffers, sodium phosphate monobasic, sodium phosphate dibasic, sodium chloride, sodium hydroxide (Sigma-Aldrich), sodium carbonate and sodium bicarbonate, tris-base, imidazole, acetic acid and hydrochloric acid (Merck) were used.

Sinapic acid (Sigma-Aldrich), FTIR grade potassium bromide (Sigma Aldrich), and deuterated chloroform ($CDCl_3$, Merck) were used for the sample preparation in MALDI-TOF mass spectroscopy, FTIR and NMR spectroscopy experiments, respectively. Spectroscopic grade trifluoroacetic acid (Sigma-Aldrich) and acetonitrile (Isolab) were employed in HPLC analyses.

All chemicals and solvents were used without any purification. Deionized water was used in the preparation of aqueous solutions.

3.2. Synthesis of SC-F127

Succinimidyl carbonate functionalized F127 (SC-F127) was prepared using the reaction in Figure 3.1. For the synthesis, 0.3 mmol of F127 was dissolved in 15 ml of dry dioxane and mixed with 4.5 mmol of DSC solution in 7.5 ml of dry acetone. Then, 4.5 mmol of DMAP dissolved in dry acetone was added dropwise to the mixture, and the mixture was stirred overnight in a magnetic stirrer in the presence of inert gas. The conjugate was isolated by precipitation with diethyl ether and centrifugation. The precipitate was dried in the fume hood, dissolved in acetone, and precipitated with diethyl ether again. This process was repeated three times. Finally, the precipitate was dissolved in deionized water, lyophilized, and stored in a refrigerator at -20°C (Huang, et al. 2002).

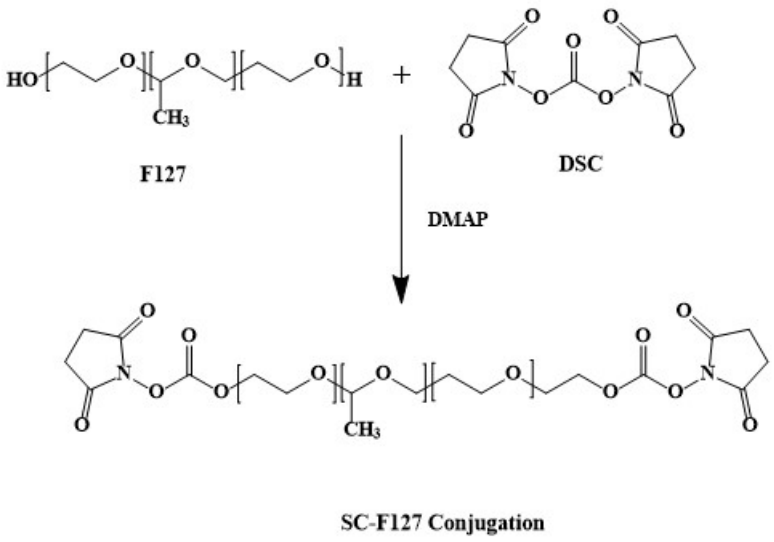

Figure 3.1. Reaction scheme of SC-F127 conjugate

3.3. Synthesis of FA-F127

Folic acid-functionalized F127 (FA-F127) was synthesized using the reaction in Figure 3.2. 1 g (0.079 mmol) F127 and 140 mg (0.32 mmol) FA were dissolved in 20 ml DMSO and stirred overnight at room temperature. Then, 0.120 g (0.32 mmol) HBTU and 0.01 g (0.082 mmol) DMAP were added to the solution and mixed on a magnetic stirrer overnight. The solution was completed to 100 ml with carbonate-bicarbonate buffer and was dialyzed against first carbonate-bicarbonate buffer, then water using a dialysis membrane (MWCO 14000 Da). Finally, the copolymers were freeze-dried and stored at -20ºC (Wu and Li 2012).

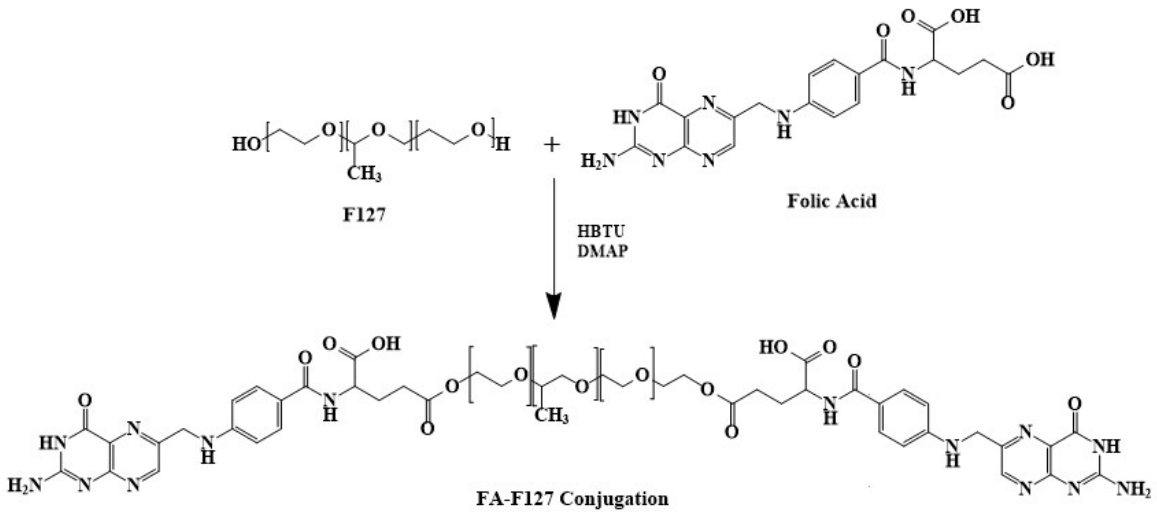

Figure 3.2. Reaction scheme of FA-F127

3.4. Solid Phase Synthesis of Peptides

All the peptides were synthesized using the Fmoc procedure on an AAPTEC Focus XI model automatic peptide synthesizer at 0.1 mmol scale. 0.127 g H-Gly-2-ClTrt resin or 0.287 g rink amide MBHA resin was used. Fmoc protecting groups at the N-terminus of amino acids were removed by treating the resin with 20% piperidine solution in DMF and DMSO (50:50) or pure DMF. A double coupling procedure was applied in the amidation reactions where DIPEA was employed as an organic base. HCTU and HATU

in DMF and DMSO (50:50) or pure DMF were used in the first and second couplings for the first five amino acids, respectively. Then, HATU was used for all couplings for the remaining amino acids. HOBt was used in the coupling of histidine to prevent racemization reactions.

After the synthesis was complete, the resin was washed with DCM and dried in a vacuum oven. Side chain protected peptide was cleaved from the 2-chlorotrityl resin using a cocktail with a composition of anisole: TFA (98:2). Deprotected peptides were obtained by treating the resin (H-Gly-2-ClTrt or rink amide MBHA resin) with a cocktail containing TFA: thioanisole: ethanedithiol: anisole (90:5:3:2). After the cleavage/deprotection reactions, the protected and deprotected peptides were isolated by precipitating on cold water and cold diethyl ether, respectively. The precipitation procedure was repeated three times. Finally, the peptides were dispersed in deionized water, lyophilized, and stored at -20^{o}C.

3.5. Synthesis of F127-Peptide Conjugates

For the conjugation of peptide and SC-F127, 20 mg (0.0125 mmol) peptide was dissolved in 10 ml DMSO, and 160 mg (0.0125 mmol) SC-F127 was added to the peptide solution in equal quantities within six hours. The reaction mixture was stirred at room temperature overnight. The unreacted peptide was removed by dialyzing the solution against deionized water for two days. Then, the copolymers were isolated by lyophilization.

3.6. Characterization of the Peptides and the Functionalized F127 Copolymers

The purity of the peptides was assessed using HPLC and MALDI-TOF mass spectroscopy methods. In the HPLC experiments, 0.1% TFA in deionized water and 0.08% TFA in acetonitrile were used as solvents A and B, respectively. 1-2 mg peptide was dissolved in 0.1 % TFA solution and filtered. Then, the sample was injected into C4 or C18 analytical columns (Inertsil WP-300, 5 μm, 4.6 × 100 mm). After the

equilibration of the column at a solvent A: solvent B ratio of 95:5, the ratio was changed to 30:70 within 65 min or to 95:5 within 75 min. The samples were eluted with a solvent flow rate of 1 ml/min, and the chromatograms were obtained by measuring the absorbance at 214 nm using a UV detector.

MALDI-TOF was used to determine the molar masses of the peptides and the F127-peptide conjugate. Samples were dissolved in 0.1 % TFA aqueous solution, and sinapic acid was used as a matrix. The analyses were conducted on a Bruker Daltonics-Autoflex III Smartbeam model MALDI-TOF-MS.

Fourier Transform Infrared (FTIR) spectroscopy or Attenuated Total Reflection (ATR) FTIR was used to determine the functional groups of the samples. For FTIR analysis, the KBr pellet technique was used. FTIR experiments were performed on a Shimadzu IRPrestige-21 FTIR-8400S model instrument. Perkin Elmer UATR Two model spectrophotometer was used in ATR-FTIR analyses.

Proton Nuclear Magnetic Resonance (1H NMR) spectroscopy was used to analyze the copolymers. Approximately 10 mg sample was dissolved into 600 µl deuterated chloroform or deuterated DMSO. The spectra were taken on a Varian Vnmr 400 model spectrometer. The data were analyzed using MestReNova software.

The degree of FA conjugation to F127 was determined using a UV-Vis spectrophotometer (Shimadzu UV-2450 model). 2.5 mg sample was dissolved in 1 ml 0.1M NaOH and diluted to the desired concentrations with 0.1 M NaOH. The degree of FA substitution was calculated using the extinction coefficient of folic acid in 0.1 M NaOH and at 282 nm, 600 L g^{-1} cm^{-1} (Sivakumar, et al. 2007).

3.7. Preparation and Characterization of Micellar Drug Delivery Systems

Curcumin was loaded to Pluronic (F127 and F127-peptide conjugate) micelles using the thin film hydration method. 1ml of 4 mg/ml curcumin solution and 2ml of 40 mg/ml Pluronic solution in DCM were mixed in a round bottom flask. The organic solvent was evaporated at 50°C, and a thin film was obtained in the flask. After that, the flasks were kept in a vacuum oven overnight at room temperature to remove DCM

completely. 4 ml pre-heated deionized water at 37°C was used to hydrate the films. Excess curcumin in the solution was removed by centrifugation at 10,000 rpm for 10 minutes (Sahu, et al. 2011).

Curcumin encapsulation and entrapment efficiency of the micelles were determined by measuring the absorbance of the samples at 435 nm. Before the absorbance measurements, curcumin-loaded samples were diluted 500 times using DMSO. The concentration of curcumin was calculated using the extinction coefficient of curcumin in DMSO at 435 nm, reported as 58547 L mol^{-1} cm^{-1} (Davis, et al. 2018). The absorbance measurements were taken on a Perkin Elmer Lambda-45 model UV-Vis spectrophotometer. Curcumin encapsulation % and entrapment efficiency % were calculated using the following equations:

$$Drug\ Encapsulation\ (\%) = \left(\frac{Amount\ of\ ancapsulated\ curcumin}{Amount\ of\ curcumin\ used}\right) x100$$

$$Entrapment\ Efficiency\ (\%) = \left(\frac{Amount\ of\ curcumin\ in\ nanocarrier}{Amount\ of\ curcumin\ loaded\ nanocarrier}\right) x100$$

Hydrodynamic diameters of the drug-loaded micelles were determined using a Malvern ZetaSizer Nano ZS model instrument via the dynamic light scattering technique. The micellar solutions prepared in deionized water (10 mg/ml) were diluted two times with 20mM phosphate buffer with 300 mM NaCl at pH 7.4 or 20mM acetate buffer with 300mM NaCl at pH 5.0. The measurements were performed within a few hours after the preparation of the solutions and after incubating the solutions for one day, two days, and three days at 37°C. The measurements were performed after equilibrating the sample for at least 5 minutes at 25°C and repeated three times. The hydrodynamic diameters of the samples were determined by applying the CONTIN method.

CHAPTER 4

RESULTS AND DISCUSSION

4.1. Characterization of the SC-F127 and FA-F127 Conjugates

pH-sensitive F127 Pluronic-peptide conjugate was prepared in three steps.

- Preparation of amine reactive F127 (SC-F127)
- pH sensitive peptide synthesis
- Conjugation of the pH sensitive peptide to SC-F127

The reaction between F127 and disuccinimidyl carbonate (DSC) in the presence of DMAP was used to prepare the succinimidyl-functionalized F127 (SC-F127). The reaction scheme is given in Figure 3.1. NMR spectra of F127 and SC-F127 are given in Figure 4.1 and Figure 4.2, respectively. Multiple broad peaks between 1.00-1.25 ppm observed in each spectrum correspond to -CH3 groups in the PPO chain, the hydrophobic part of the F127 copolymer. Broad peaks between 3.30-3.50 ppm indicate the chemical shifts of backbone protons of F127. The newly formed peaks between 2.83-2.87 ppm in the SC-F127 spectrum are related to the protons of the succinimidyl group (-COON-$(CO)_2(CH_2)_2$) of SC-F127 (Huang, et al. 2002). These peaks prove that the succinimidyl group is conjugated to the copolymer.

FTIR spectra of F127, DSC, and SC-F127 samples are presented in Figures 4.3a, 4.3b, and 4.3c, respectively. The bands observed at 2887 cm^{-1} and 1112 cm^{-1} in both FTIR spectra are due to the stretching vibrations of the -C-H and -C-O-C- groups in F127. The strong band at about 1700 cm^{-1} in the spectrum of DSC corresponds to the -C=O vibrations of the succinimidyl groups. This band appears in the FTIR spectrum of SC-F127 at ~1717 cm-1, indicating the presence of the carbonyl group. Thus, NMR and FTIR results confirm that the succinimidyl form of F127 was successfully synthesized,

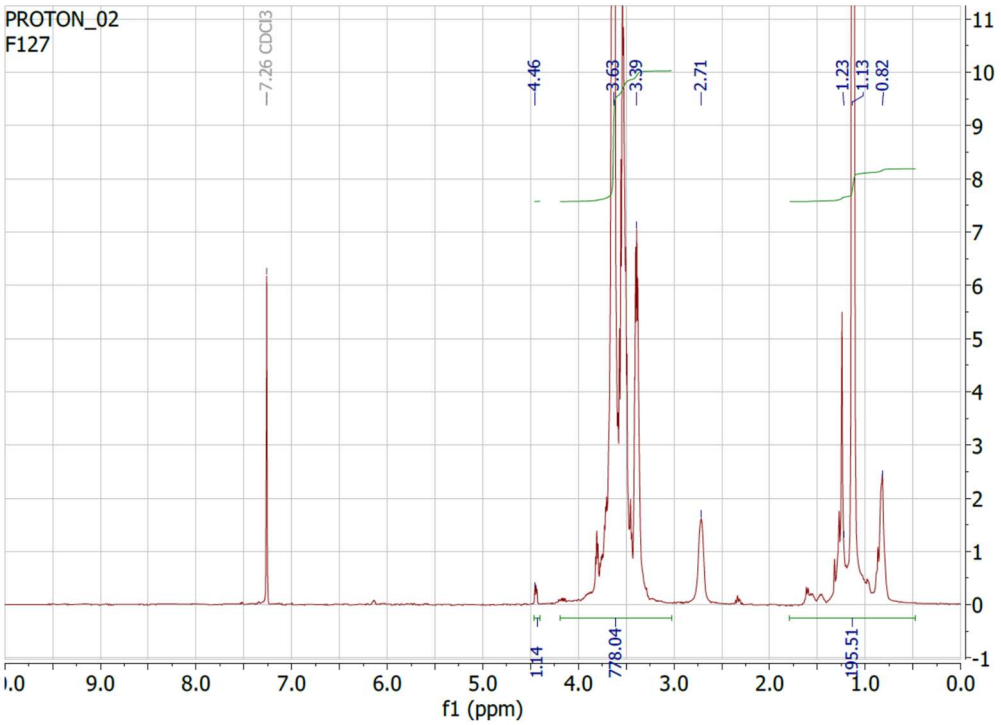

Figure 4.1. NMR Spectrum of F127

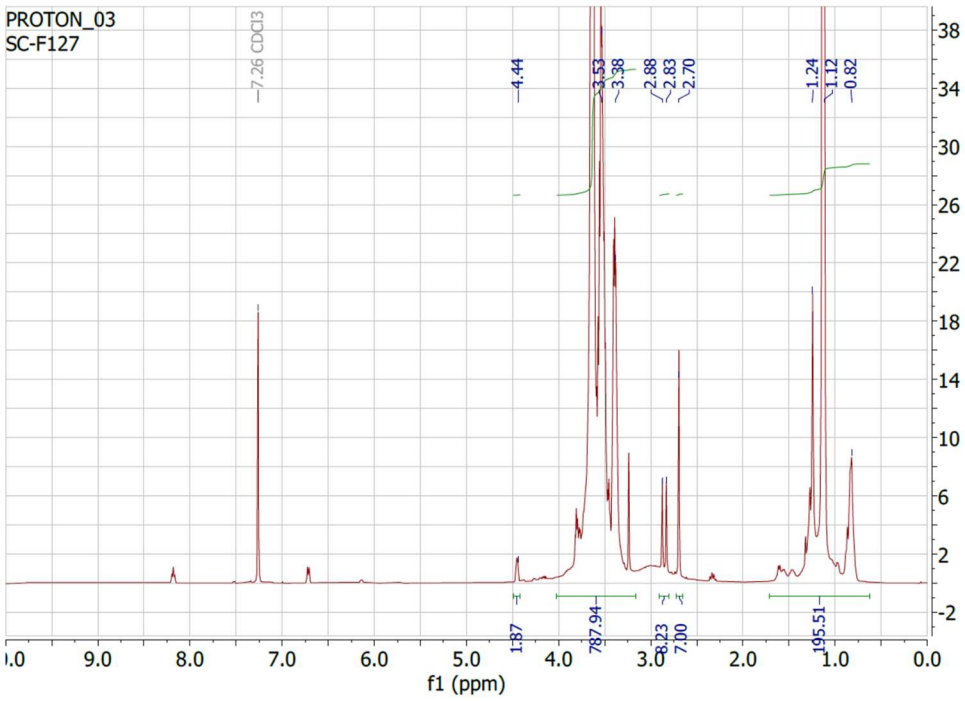

Figure 4.2. NMR spectrum of SC-F127

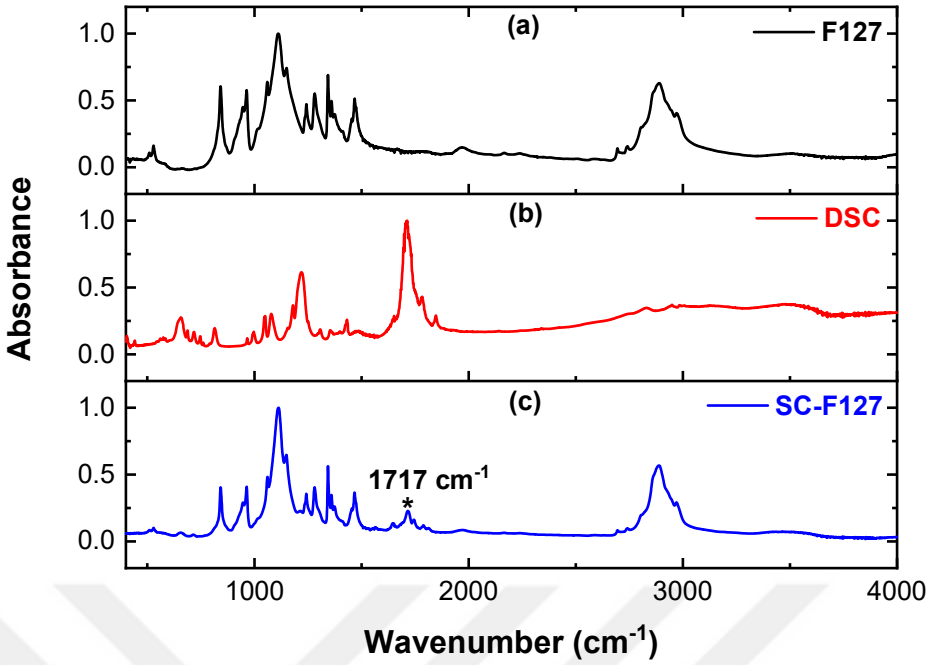

Figure 4.3. FTIR spectra of a) F127, b) DSC, and c) SC-F127

F127 was conjugated with folic acid to impart active targeting to the curcumin carrier system. The reaction scheme is presented in Figure 3.2. The FTIR spectrum of the obtained copolymer (FA-F127) is shown in Figure 4.4b. There was not much difference between the FTIR spectrum of FA-F127 and F127. The stretching band of -C=O groups expected to be observed around 1700 cm^{-1} was not observed in the FA-F127 spectrum. However, vibrations of the -N-H groups of folic acid were observed indistinctly in the region of about 1600 cm^{-1}. The FA conjugation was more precisely determined in the ^{1}H NMR spectrum of FA-F127 in Figure 4.5. The peaks above 8.60 ppm, 6.60 ppm, and 7.60 ppm in the ^{1}H NMR spectrum of the FA-F127 conjugate are due to chemical shifts of the aromatic groups in the pterin group and p-amino benzoate group of folic acid, respectively.

UV-Vis spectrum was used to determine the degree of folic acid functionalization quantitatively. UV Spectra of F127, folic acid, and FA-127 are given in Figure 4.6. F127 did not show any peak. The spectra of folic acid and FA-F127 are very similar. Using the absorbance value corresponding to the wavelength of 282 nm of FA-F127 and the extinction coefficient of folic acid, folic acid conjugation was calculated as 30% per F127 chain.

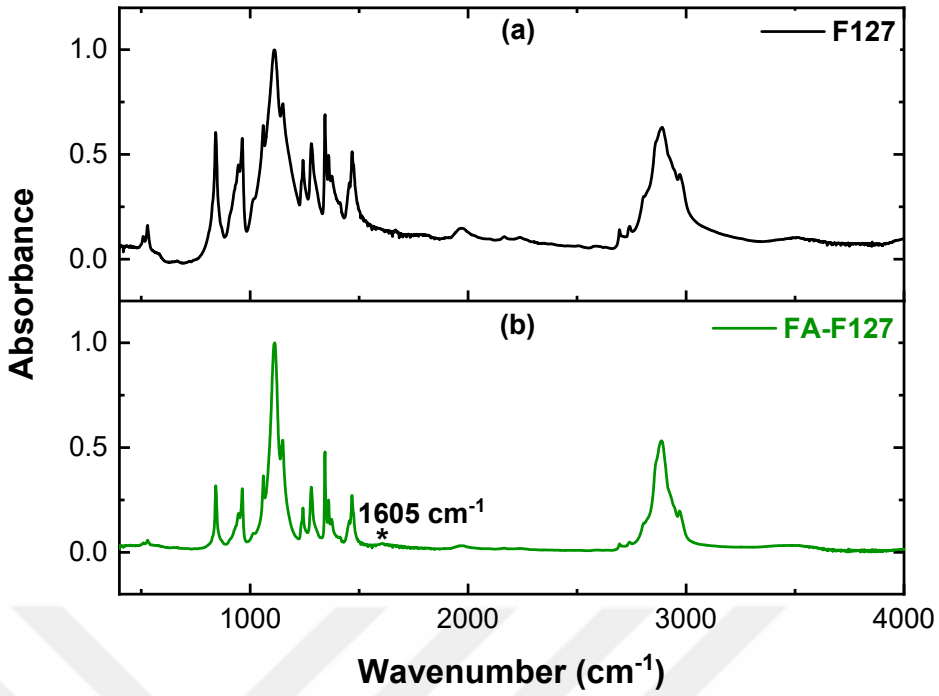

Figure 4.4. FTIR Spectrum of a) F127 and b) FA-F127

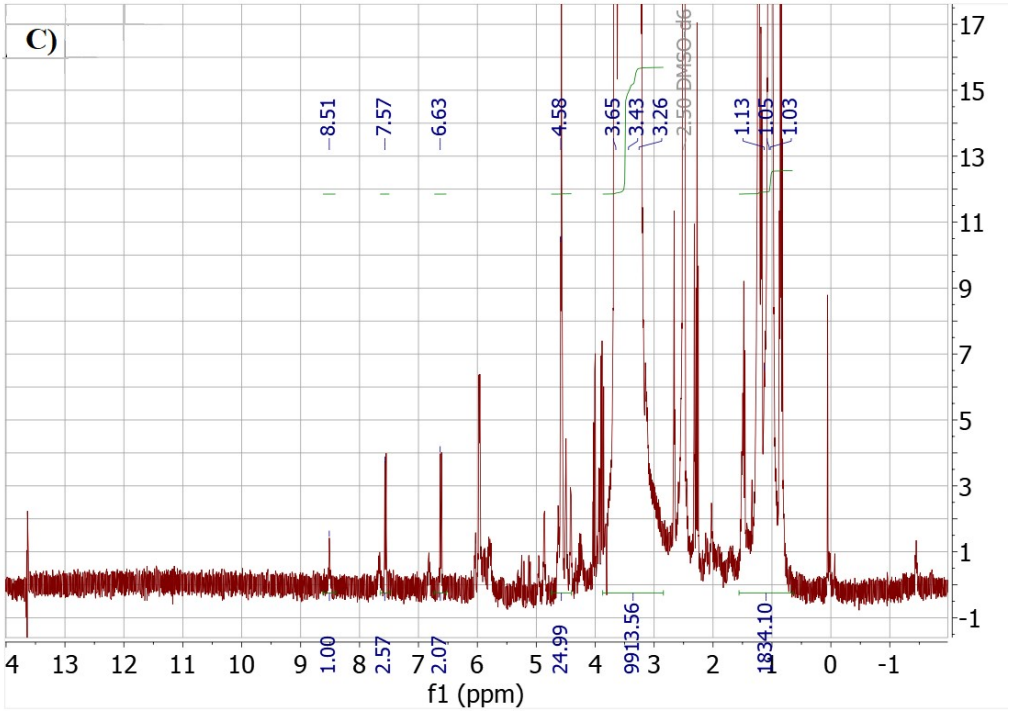

Figure 4.5. NMR Spectrum of FA-F127

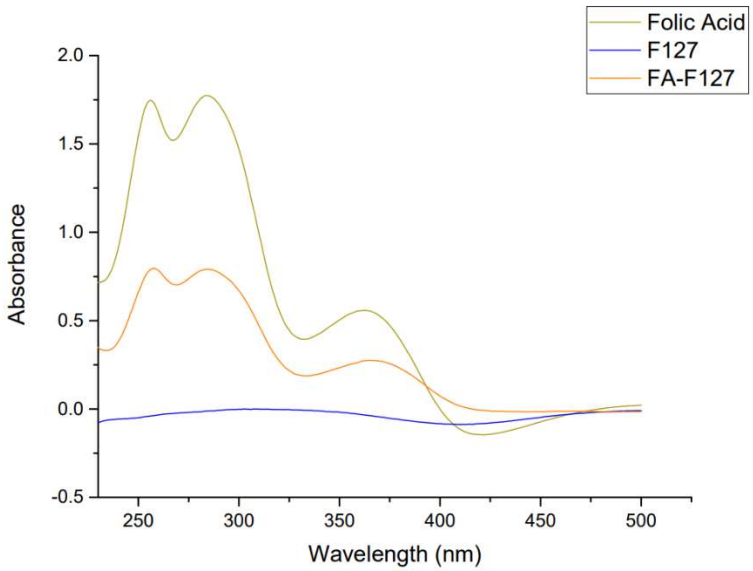

Figure 4.6. UV-Vis spectra of Folic Acid, F127 and FA-F127

4.2. Characterization of the Peptides and the Peptide-F127 Conjugates

The peptides synthesized in this study were designed to have multiple histidine moieties to impart pH responsiveness to the drug delivery system. In some sequences, GFWFG sequence was used as the endosome disruptive domain. The drug delivery system was obtained by conjugating the pH-responsive peptide to an amine-reactive SC-F127 copolymer. To obtain high purity of functional peptide, different resins and solvents were used, and peptide sequences were changed. Side chain-protected peptides were synthesized using H-Gly-2-ClTrt resin, whereas rink amide MBHA resin gave deprotected peptides. Pure DMF and 50:50 DMF:DMSO mixture were used as solvents. Sequences, theoretical molar masses, and the synthesis conditions of the peptides investigated in this study are given in Table 4.1.

The purity of the peptides was determined using HPLC and MALDI-TOF mass spectroscopy. HPLC curves of the peptides synthesized using H-Gly-2-ClTrt resin (peptide 1, peptide 2, and peptide 3) are given in Figures A1, A2, and A3. MALDI-TOF mass spectra of peptide 1, peptide 2, and peptide 3 are presented in Figures 4.7, 4.8, and 4.9, respectively.

Table 4.1. Properties and Synthesis Conditions of the Peptides

Notation	Resin	Solvent	Sequence	Molar Mass (Da)
peptide-1	H-Gly-2-ClTrt	DMF-DMSO	$GGH_{13}GGFWFGGSG$	2767.8
peptide-2	H-Gly-2-ClTrt	DMF-DMSO	$GGGH_{13}GGSG$	2173.2
peptide-3	H-Gly-2-ClTrt	DMF	$GGHGH_2QH_2QH_3QH_3GGSG$	2340.4
peptide-4	Rink amide MBHA	DMF-DMSO	GGH_6GFWFG	1548.7

HPLC curve of the peptide-1, taken using a C18 column, has a single peak at 24 min suggesting high purity of peptide-1 was synthesized. However, in its MALDI-TOF spectrum, along with the peak corresponding to the theoretical molar mass of the peptide (2767.8 Da), lower molar mass peaks with higher intensities were also observed (Figure 4.7). These lower molar mass peptide fractions were obtained in the peak positions corresponding to multiples of 137 Da less than the theoretical molar mass of the peptide. This result indicates that histidine residues were not effectively incorporated into the peptide sequence. Additionally, it is likely that the C18 column cannot resolve peptides with different molar masses.

In the design of peptide 2, the hydrophobic endosome disruptive unit was removed. MALDI-TOF mass spectrum presents the theoretical molar mass of the peptide-2 (2174.1 Da). Similar to peptide-1, in addition to the designed peptide sequence containing 13 histidines, those with 12, 11, 10, 9, 8, 7, 6, and 5 histidines were also identified (Figure 4.8). These fractions were also observed in the HPLC results obtained with the C4 column.

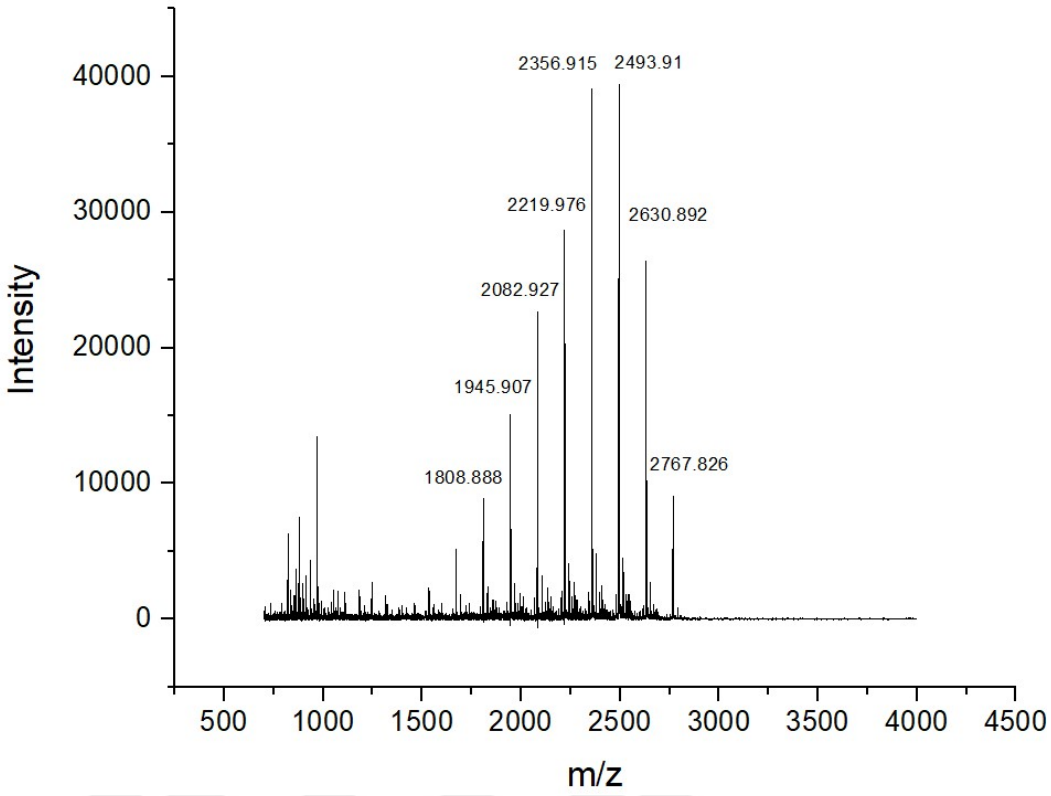

Figure 4.7. MALDI-TOF Mass Spectrum of Peptide-1

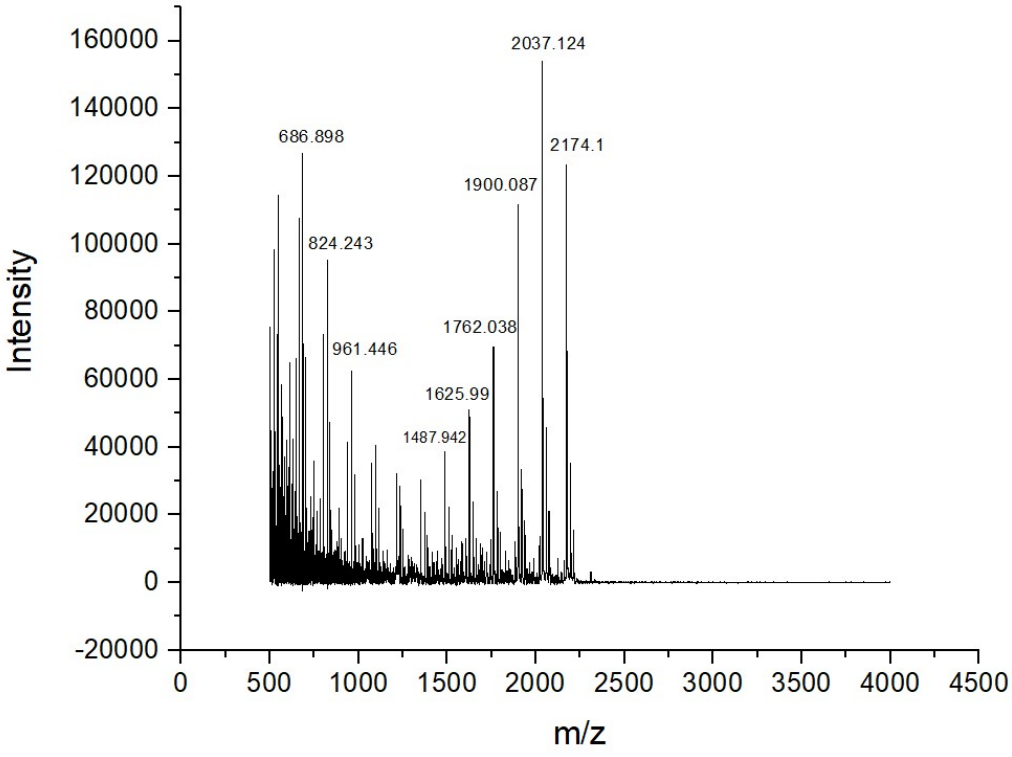

Figure 4.8. MALDI-TOF Mass Spectrum of Peptide-2

Peptide-3 was designed to have glutamines between histidines to overcome the difficulties in the incorporation of adjacent histidines. The endosome disruptive domain was not used in the peptide-3 sequence. Instead of DMF and DMSO mixture, pure DMF was used in the synthesis to improve the swelling ratio of the resin. Compared to peptide-1 and peptide-2, peptide-3 was synthesized in higher purity. The HPLC curve in Figure A.3 indicates that peptide-3 eluted as a single peak. However, the peptide sequences with missing histidines were also observed in the MALDI-TOF spectrum (Figure 4.9). These results suggest that the high-loading 2-chlorotrityl resin is unsuitable for the sequences with adjacent histidines. Although synthesis of the side-chain protected peptides would be advantageous to prevent possible side reactions during the peptide and F127 conjugation, the purity of the resultant peptide can be a concern. For this reason, we switched to a low-loading rink amide resin and designed a shorter peptide, peptide-4.

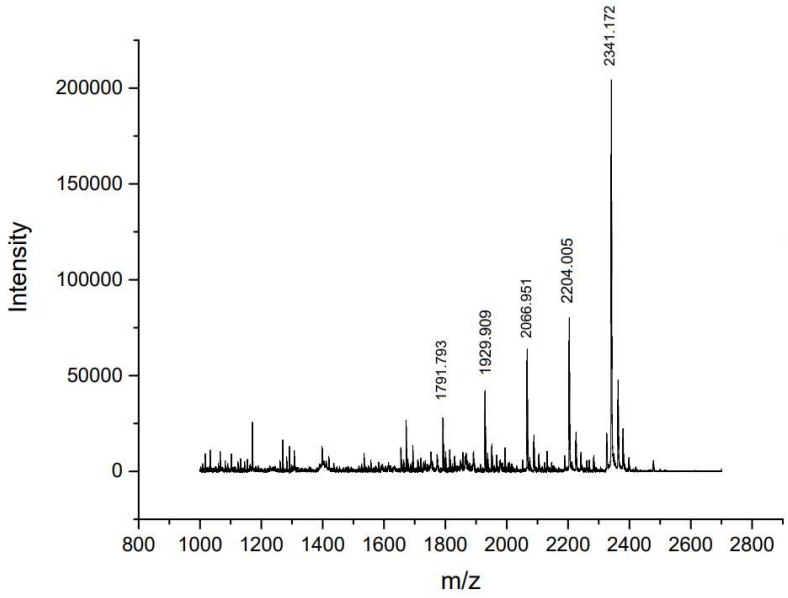

Figure 4.9. MALDI-TOF Mass Spectrum of Peptide-3

MALDI-TOF mass spectrum of peptide-4 indicates Na+ and K+ adducts observed at 1570.6 Da and 1586.6 Da, along with H+ adduct at 1548.6 Da (Figure 4.10). The intensity of the other peaks is relatively low, showing the high purity of peptide with a small amount of shorter peptide sequences. For this reason, peptide-4 was selected to conjugate to SC-F127.

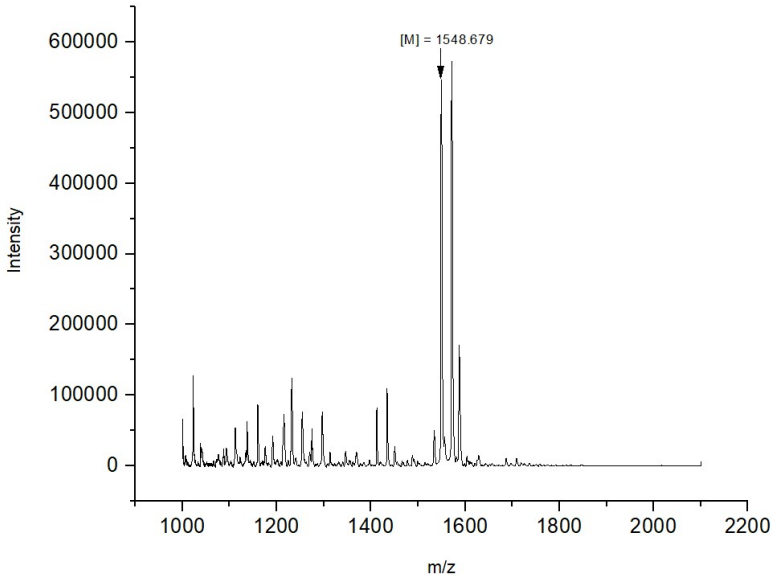

Figure 4.10. MALDI-TOF Mass Spectrum of Peptide-4

Peptide-4 has six histidines and the endosome disruption unit. The curcumin carrier system was obtained by the reaction between the peptide-4 and amine-reactive SC-F127. ATR-FTIR spectrum of the resultant F127-peptide conjugate is given in Figure 4.11. In this spectrum, carbonyl group vibrations at ~1700 cm-1 disappeared, and a new band at about 1650 cm-1 due to the -N-H vibrations of the peptide bond was observed (Balcı and Top 2018). MALDI-TOF spectrum of the F127-peptide conjugate, a broad peak between 12000 Da and 20000 Da was observed due to the polydispersity of F127 (Figure 4.12). The peak centered at 14857 Da is very close to the theoretical molar mass (12600 Da + 1548.7 Da = 14148.7 Da), confirming the conjugation of peptide to the F127 copolymer. The data also suggest the conjugation of one peptide molecule to the one end of F127. There might be conjugates with two peptides attached to both ends of F127. However, the broadness of the MALDI-TOF spectrum obscured the resolution of the conjugates with two peptides and the unconjugated F127 species. Nevertheless, along with the FTIR spectrum, the MALDI-TOF mass spectrum of the sample indicates at least contains F127-peptide species. We have used Ni-NTA column purification to remove unreacted F127, but these purified species could not be thoroughly dissolved in DCM n the curcumin loading process (data not shown).

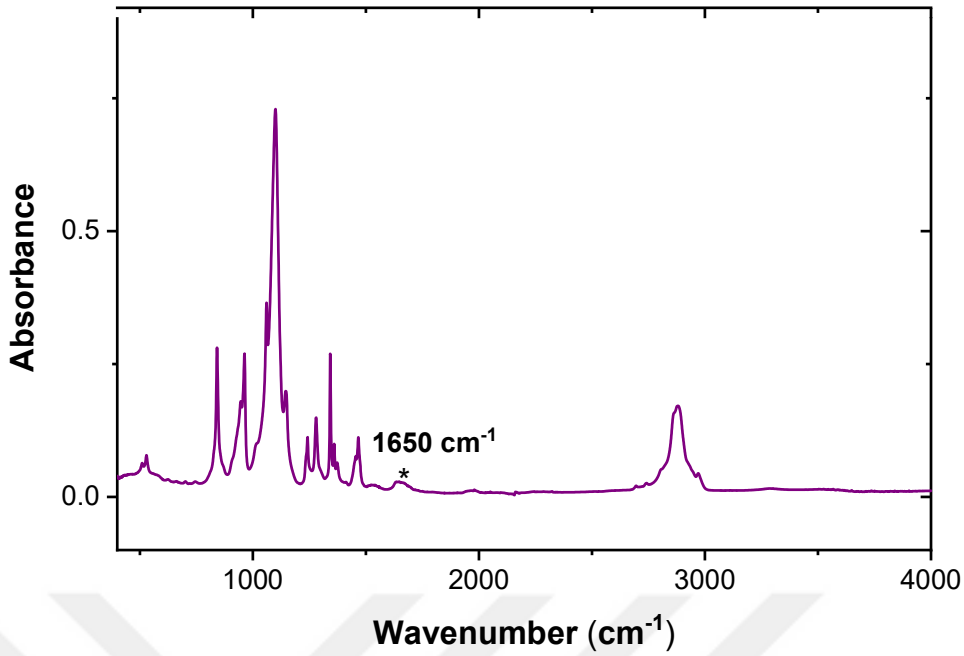

Figure 4.11. ATR-FTIR spectrum of F-127-peptide conjugate

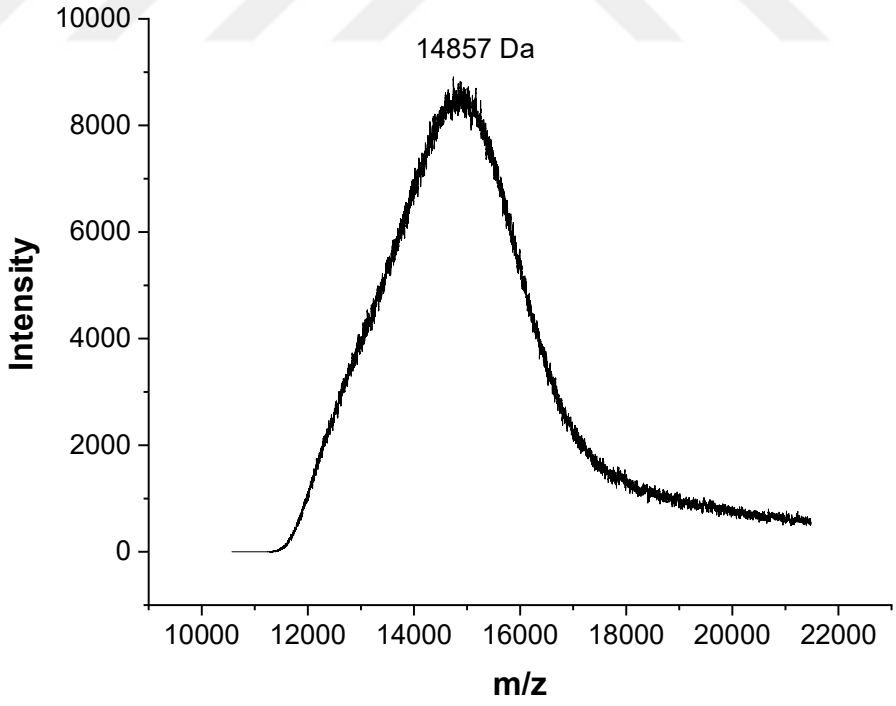

Figure 4.12. MALDI-TOF mass spectrum of F127-peptide conjugate

4.3. Characterization of the Drug Delivery System

Curcumin-loaded F127 and F127-peptide conjugate micelles were prepared using the thin film method. Curcumin encapsulation % and entrapment efficiency % of the micelles are summarized in Table 4.2. The copolymer itself has quite a high drug-loading capacity. Almost all the curcumin was incorporated into F127 micelles. However, the drug loading capacity of F127-peptide conjugate is lower. The F127-peptide conjugate has hydrophobic amino acids such as tryptophane and phenylalanine. Thus, the conjugate-based drug delivery system is expected to have a higher drug encapsulation % and entrapment efficiency %. However, peptide conjugation decreased the solubility of F127 in DCM. For this reason, drug loading to these micelles has become difficult.

Table 4.2. Drug Encapsulation % and Entrapment Efficiency % of F127 and F127-peptide conjugate

Sample	**Entrapment Efficiency (%)**	**Drug Encapsulation (%)**
F127	101 ± 4	4.83 ± 0.36
F127-peptide conjugate	86 ± 1	4.10 ± 0.02

Dynamic light scattering was used to determine the stability and size distributions of the drug delivery systems at pH 5.0 and 7.4. For empty F127 micelles, D50 values based on number distribution were obtained as 11.5 ± 0.9 nm and 11.9 ± 0.5 nm at pH 7.4 and pH 5.0, respectively. Size distributions of curcumin-loaded F127 and F127-peptide conjugate obtained in different time intervals and at different pH values are given in Figures 4.13-4.24. respectively. In number-based size distributions, a single peak between 10 and 30 nm was observed independent of pH for both samples. The peak position did not change as the sample was incubated at different intervals. However, the presence of the aggregates was detected in the intensity-based size distribution data. Initially, both samples have bidisperse size populations for the first two days independent of pH. On day 3, the size distribution of the curcumin-loaded F127 sample reveals the third population above 1000 nm at both pH values. However,

for the curcumin-loaded F127-peptide sample, the third peak was observed only at pH 5.0 on days 2 and 5, suggesting the pH sensitivity of this sample. Thus, the time course aggregation of the samples is likely related to the curcumin release to the environment.

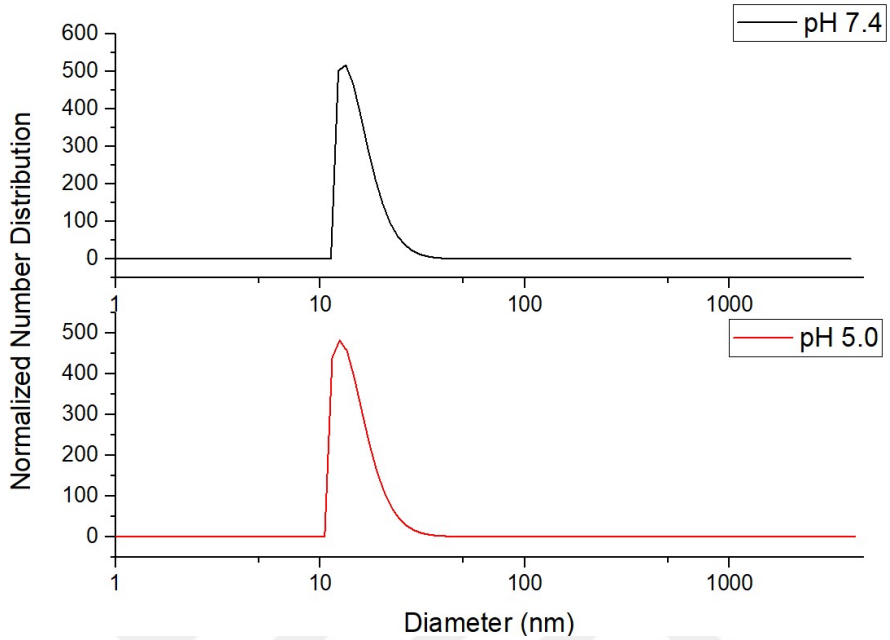

Figure 4.13. Number based size Distribution of Curcumin loaded F127 at day 1

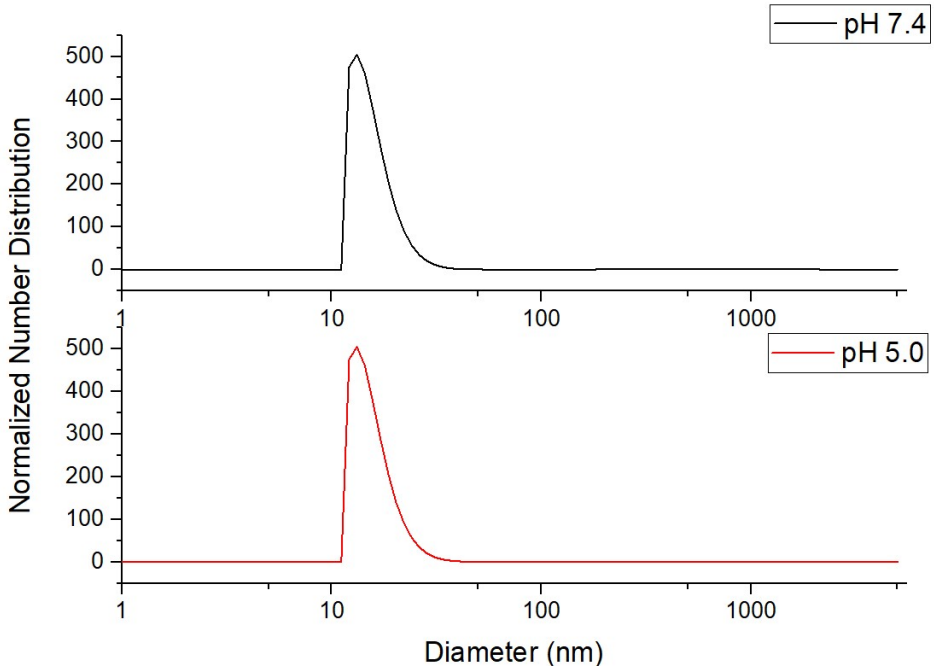

Figure 4.14. Number based size Distribution of Curcumin loaded F127 at day 2

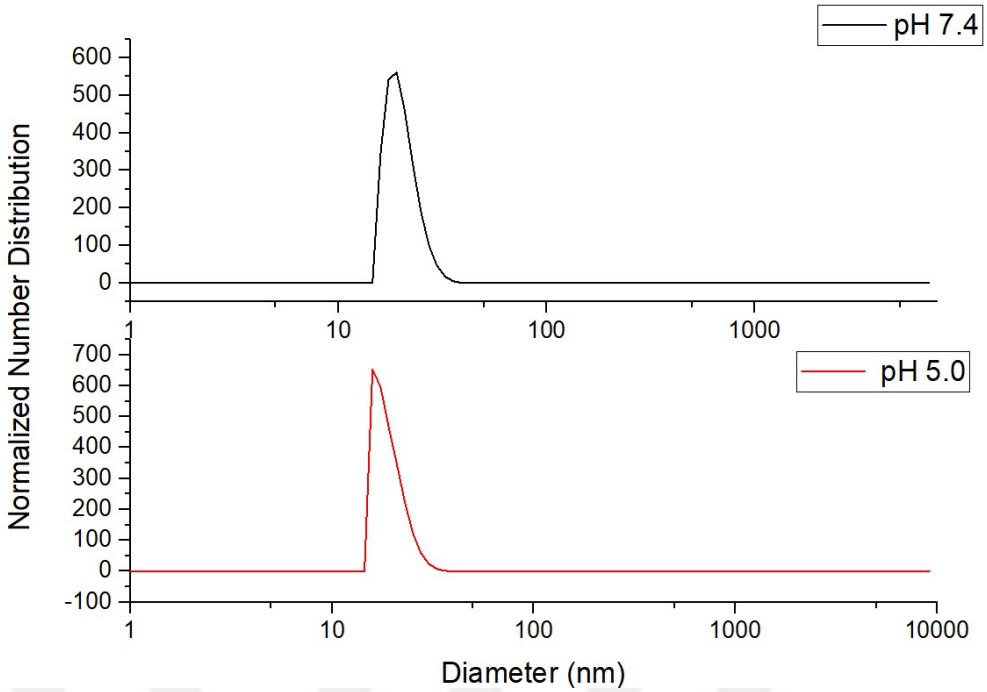

Figure 4.15. Number based size Distribution of Curcumin loaded F127 at day 3

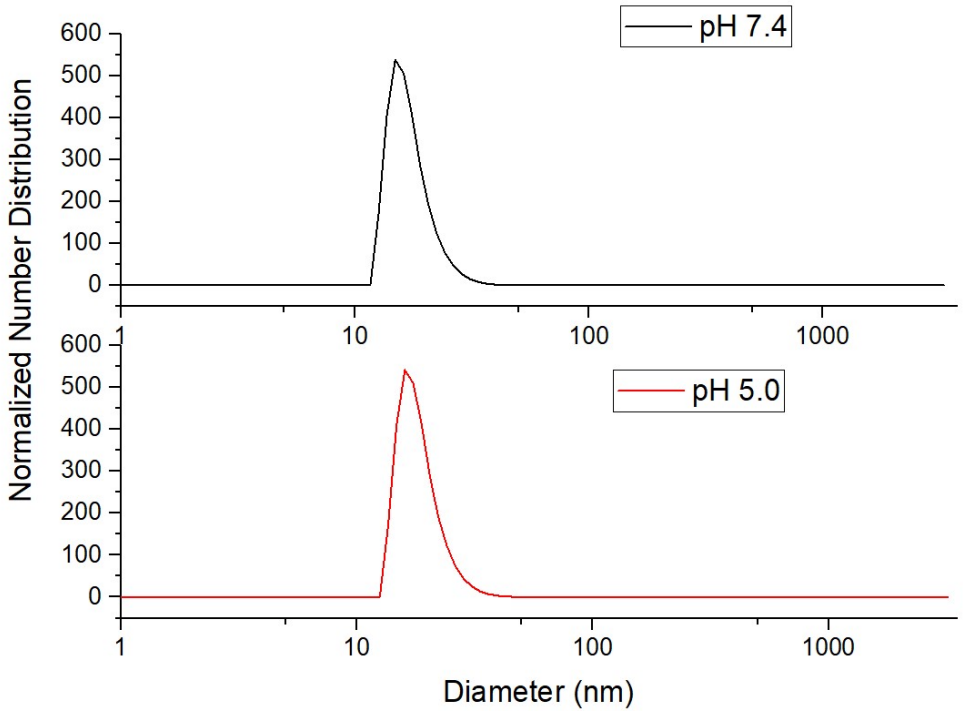

Figure 4.16. Number based size Distribution of Curcumin Encapsulated Peptide-F127 Conjugate at day 1

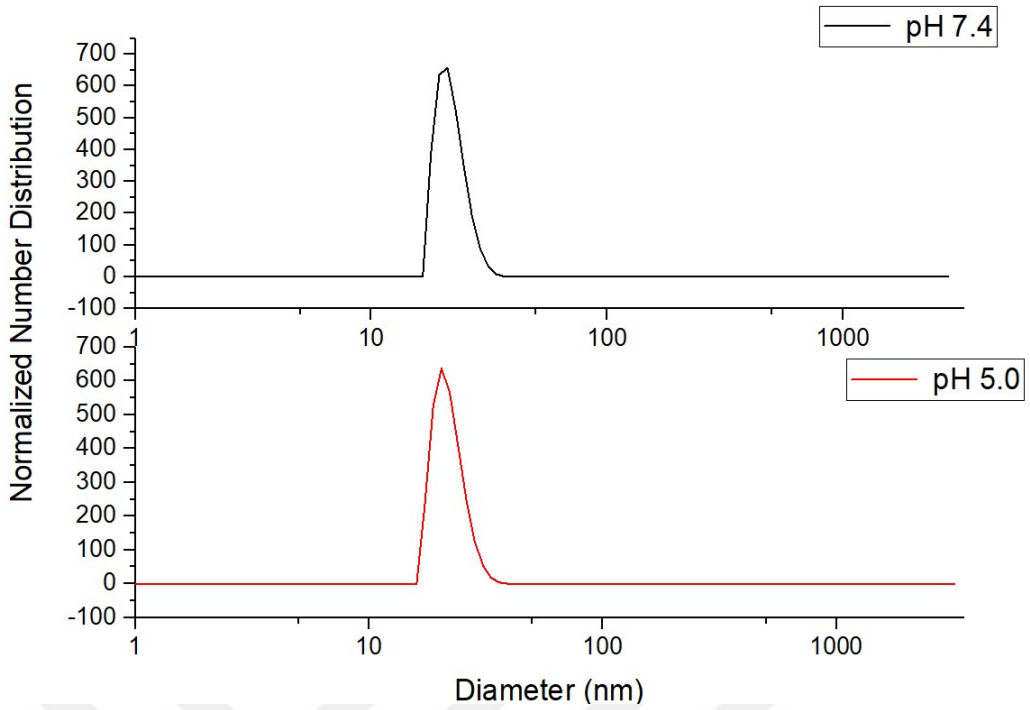

Figure 4.17. Number based size Distribution of Curcumin Encapsulated Peptide-F127 Conjugate at day 2

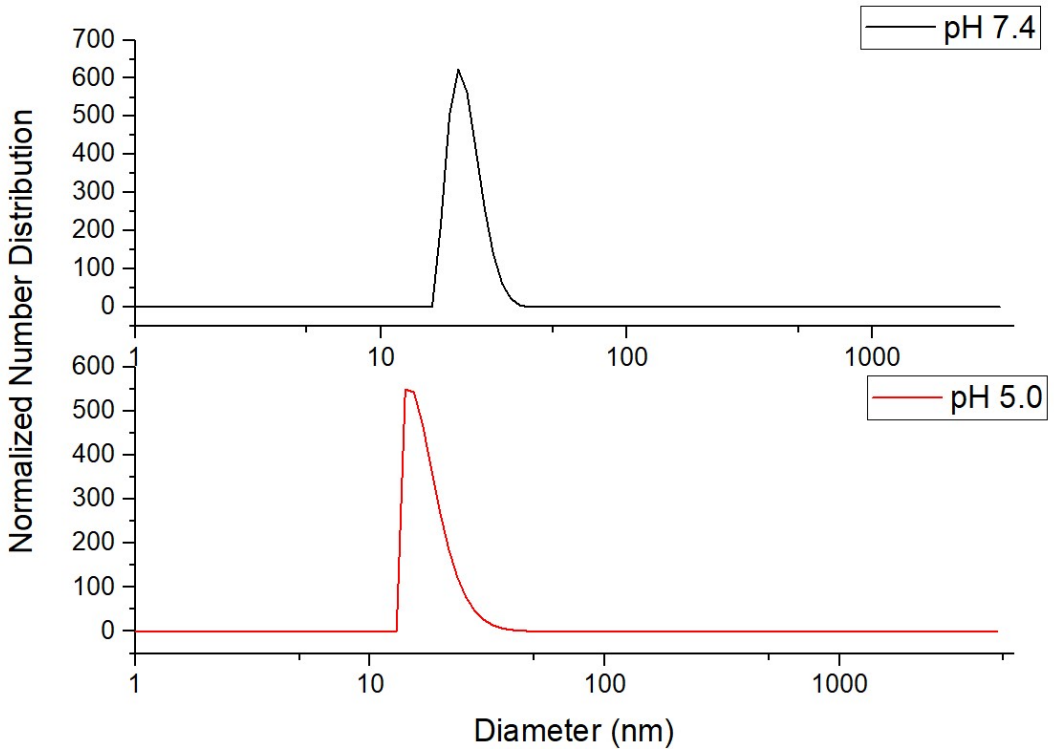

Figure 4.18. Number based size Distribution of Curcumin Encapsulated Peptide-F127 Conjugate at day 5

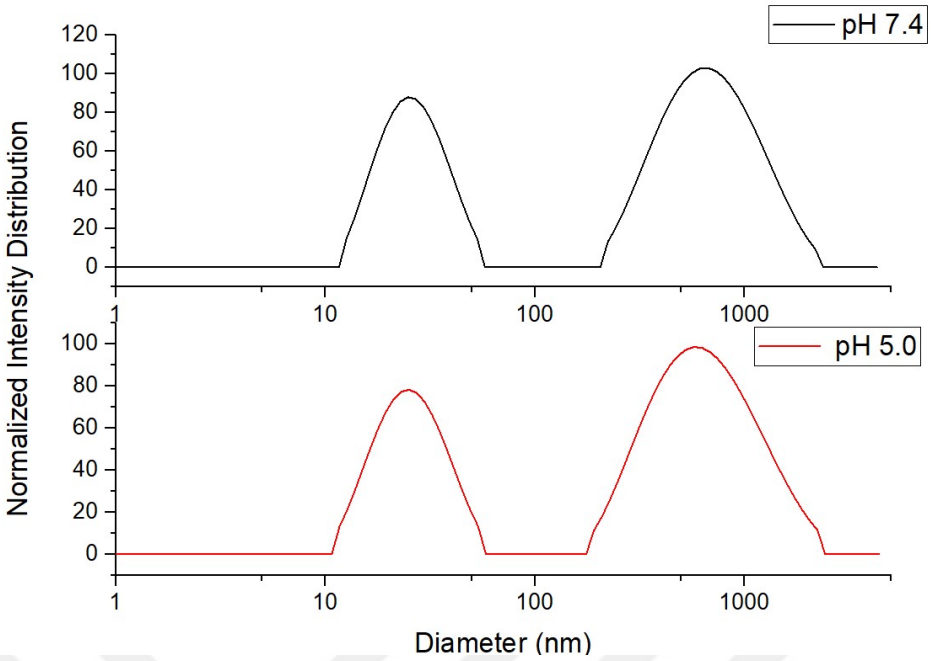

Figure 4.19. Intensity based size Distribution of Curcumin loaded F127 at day 1

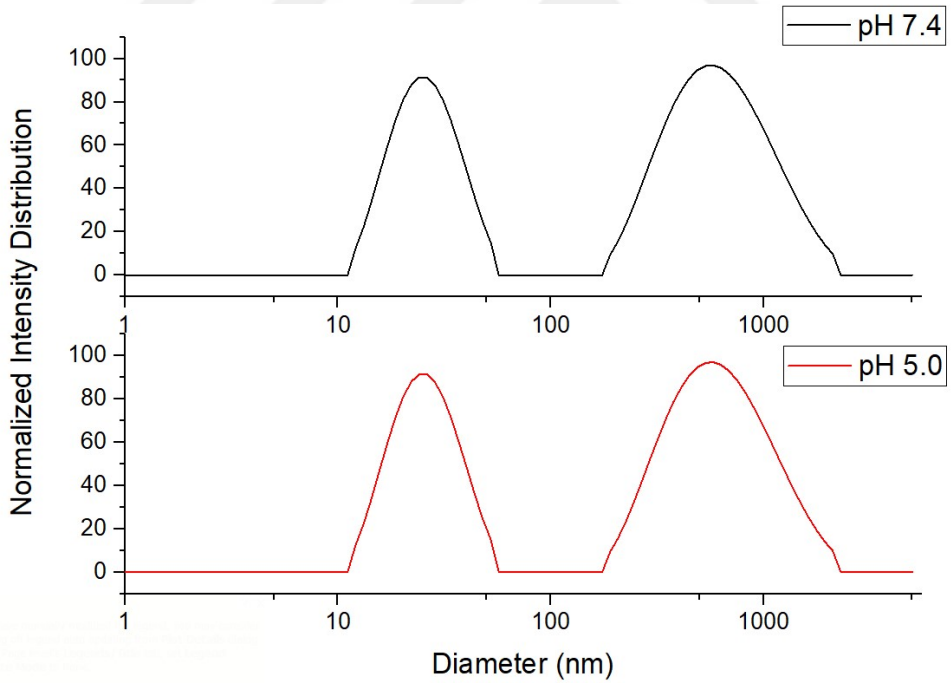

Figure 4.20. Intensity based size Distribution of Curcumin loaded F127 at day 2

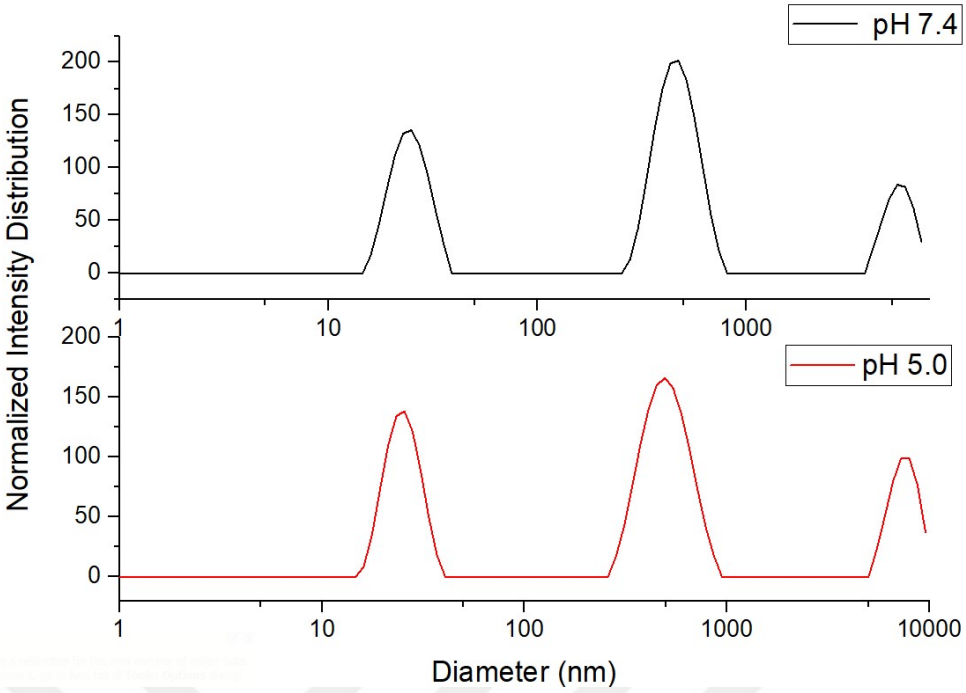

Figure 4.21. Intensity based size Distribution of Curcumin loaded F127 at day 3

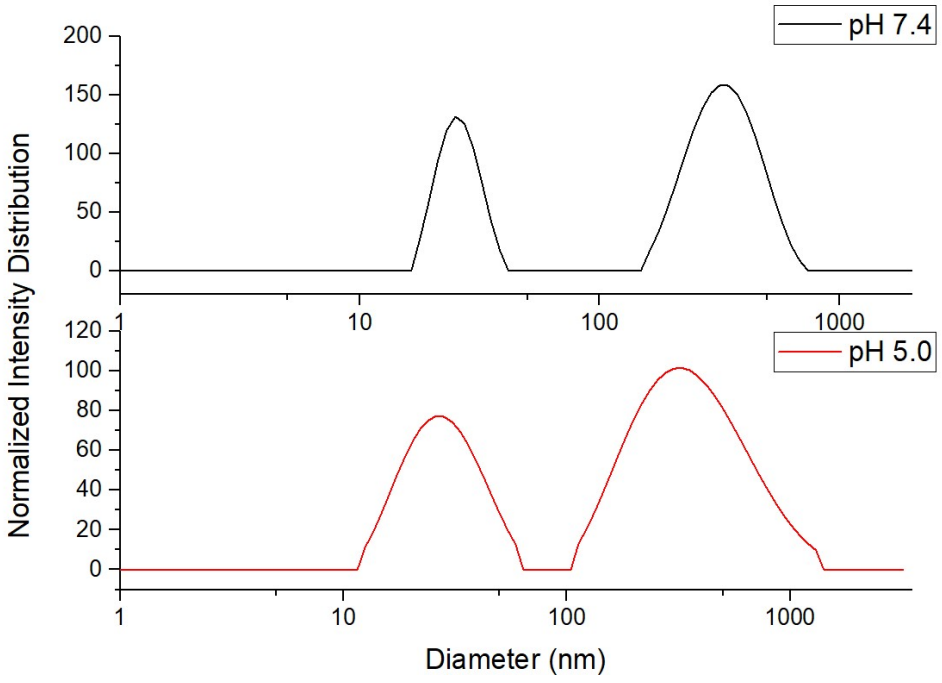

Figure 4.22. Intensity based size Distribution of Curcumin Encapsulated Peptide-F127 Conjugate at day 1

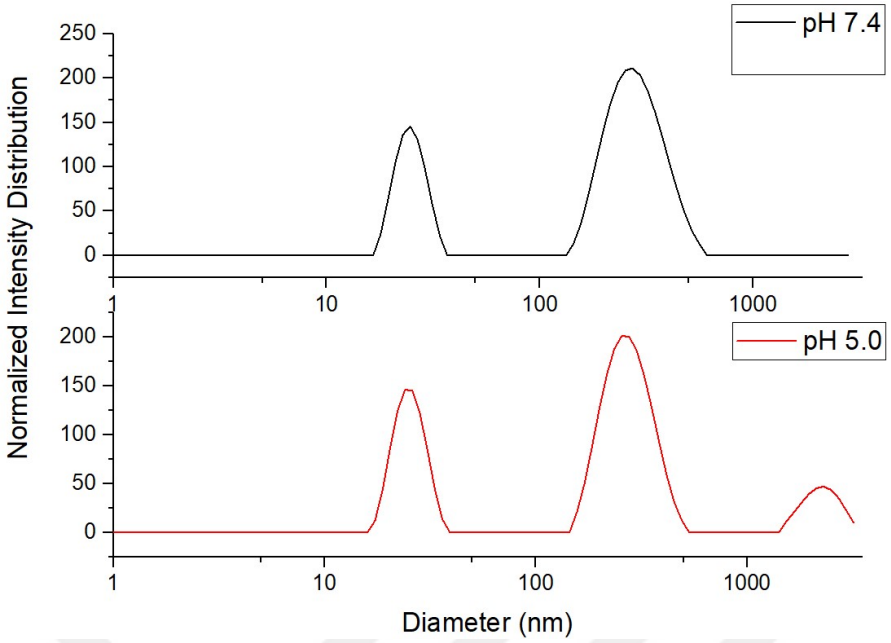

Figure 4.23. Intensity based size Distribution of Curcumin Encapsulated Peptide-F127 Conjugate at day 2

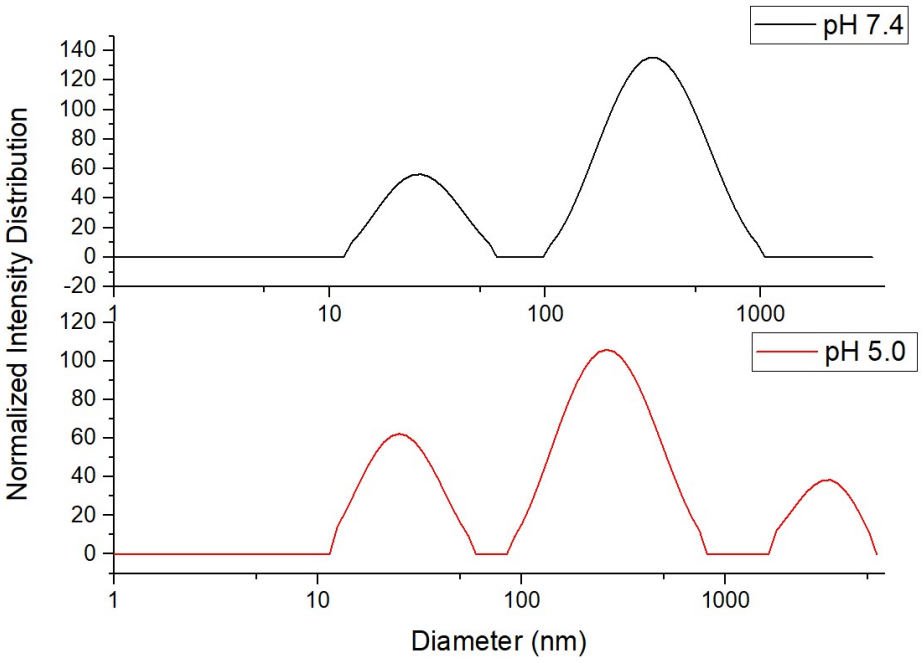

Figure 4.24. Intensity based size Distribution of Curcumin Encapsulated Peptide-F127 Conjugate at day 5

CHAPTER 5

CONCLUSIONS AND FUTURE WORK

This study focuses on synthesizing and preliminary characterization of a curcumin delivery system based on a Pluronic F127-peptide conjugate. In this system, curcumin and F127 were selected as they were reported to have the potential to reverse multidrug resistance. The peptide was designed to contain pH-responsive histidines and endosome disruptive GFWFG sequence. Curcumin was loaded to the F127 and F127-peptide conjugate. Entrapment efficiency %, stabilization, and pH responsiveness of the curcumin-loaded micellar systems were investigated. Almost all curcumin was incorporated into the F127 micelles. However, F127-peptide micelles exhibited lower entrapment efficiency % due to the decrease in the solubility of the conjugate in DCM. Number-based size distribution of the micelles indicates a single-size population between 10 and 30 nm independent of pH and incubation time. However, the aggregation tendency of both micelles and the pH-responsive behavior of F127-peptide were resolved by the intensity-based size distribution data.

In conclusion, histidine-containing F127 conjugates can be a promising curcumin delivery system due to the pH responsiveness and potential multidrug resistance reversal properties. However, curcumin release properties and cytotoxicity of the carrier systems against drug-resistant cancer cells should be evaluated. The solubility problem of the conjugate system can be solved by changing the peptide sequence. Additionally, active targeting can be imparted to the carrier system by preparing the mixed micellar system of folic acid functionalized F127 (FA-F127) and F127-peptide conjugate.

APPENDIX A

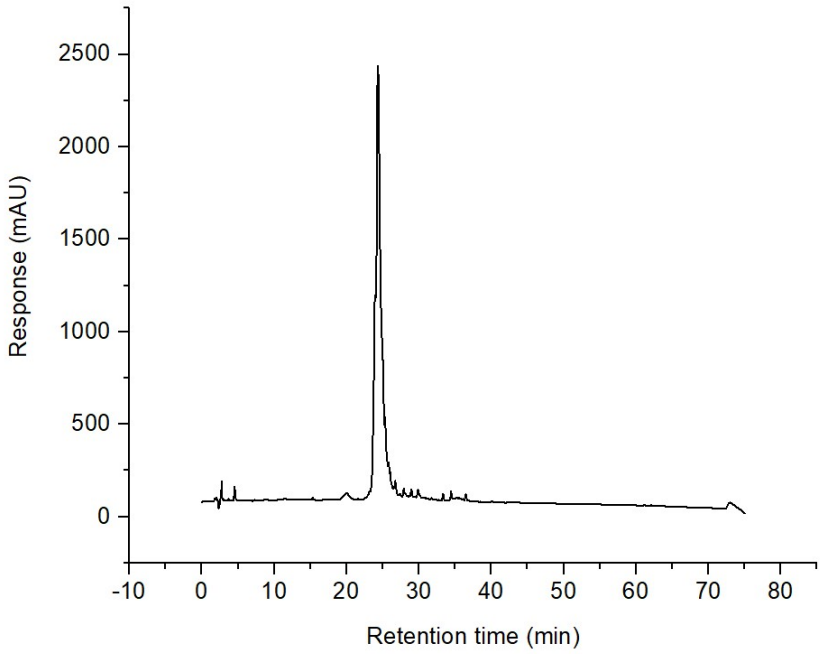

Figure A.1. HPLC chromatogram of Peptide-1

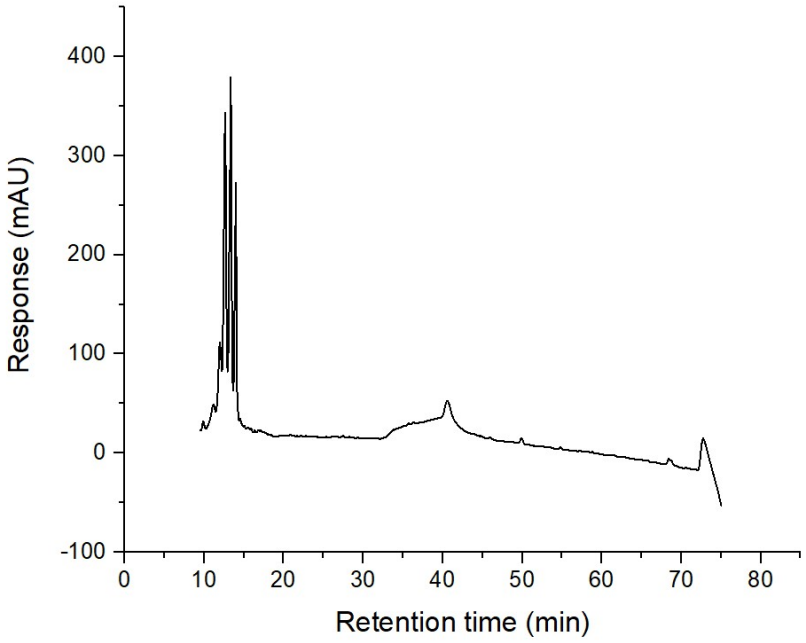

Figure A.2. HPLC Chromatogram of Peptide-2

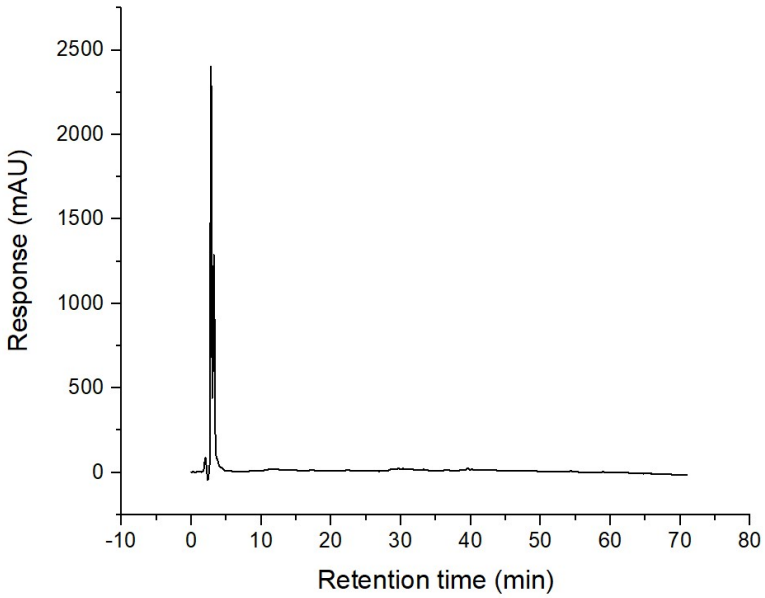

Figure A.3. HPLC Chromatogram of Peptide-3

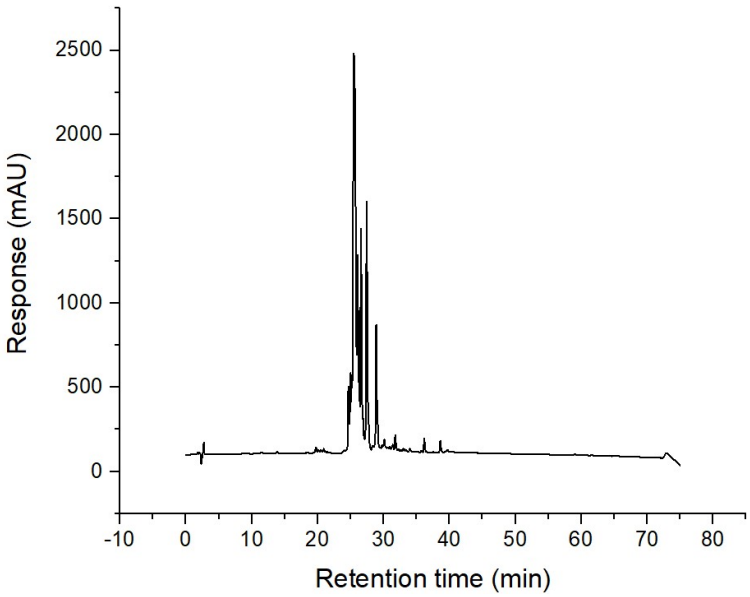

Figure A.4. HPLC Chromatorgam of Peptide-4

REFERENCES

Abdalla, Ahmed M.E. , Lin Xiao, Muhammad Wajid Ullah, Miao Yu, Chenxi Ouyang, and Guang Yang. "Current Challenges of Cancer Anti-angiogenic Therapy and the Promise of Nanotherapeutics." *Theranostics* 8, no. 2 (2018): 533-548.

American Cancer Society. March 2021. https://www.cancer.org/cancer/cancer-basics/history-of-cancer/what-is-cancer.html (accessed 03 16, 2021).

Balcı, Beste, and Ayben Top. "PEG and PEG-Peptide Based Doxorubicin Delivery Systems Containing Hydrazone Bond." *Journal of Polymer Research*, October 2018: 1-12.

Baran, Yusuf. *Kanser Moleküler Biyolojisi.* İzmir: Kısayol Yayıncılık, 2018.

Batrakova, Elena V. , and Alexander V. Kabanov. "Pluronic Block Copolymers: Evolution of Drug Delivery Concept From Inert Nanocarriers To Biological Response Modifiers." *Journal of Controlled Release*, 2008: 98-106.

Boss, Silvan D., and Simon Mensah Ametamey . "Development of Folate Receptor−Targeted PET Radiopharmaceuticals for Tumor Imaging—A Bench-to-Bedside Journey." *Cancers* 12, no. 1508 (2020): 1-20.

Britannica, The Editors of Encyclopaedia. 12 04, 2022. https://www.britannica.com/science/macromolecule.

Burgio, Ernesto, ve Lucia Migliore. «Towards a Systemic Paradigm in Carcinogenesis: Linking Epigenetics and Genetics.» *Molecular Biology Reports* 42, no. 4 (2014): 777-790.

Chen, Chen, et al. "Structural Basis For Molecular Recognition of Folic Acid by Folate Receptor." *Nature*, 2013: 1-5.

Cooper, Geoffrey M. *The Cell: A Molecular Approach 2. Edition.* Sunderland: Sinauer Associates, 2000.

Çiftçi, Nihal. "The Role of Oxidative Stress in Cancer: Could Antioxidants Fuel the Progression of Cancer." *Ahi Evran Tıp Dergisi*, 2017: 8-13.

Davis, Benjamin M., et al. "Topical Curcumin Nanocarriers are Neuroprotective in Eye Disease." *Scientific Reports*, July 23, 2018: 1-13.

Encyclopedia Brittanica. 2021. https://www.britannica.com/biography/William-Henry-Perkin (accessed 11 26, 2020).

Fang, Xiao-Bin , et al. "F68-Curcumin Conjugates For Improved Tumor Intracellular Drug Delivery." *International Journal of Pharmaceutics* 502, no. 1-2 (2016): 28-37.

Galmarini, Darío , Carlos M. Galmarini, ve Felipe C. Galmarini. «Cancer Chemotherapy: A Critical Analysis of Its 60 Years of History.» *Critical Reviews in Oncology/Hematology*, 2012: 181-199.

Ghalehkhondabi, Vahab, Alireza Fazlali, and Meysam Soleymani. "Folic Acid-Conjugated pH-Responsive Poly(methacrylic acid) Nanospheres For Targeted Delivery of Anticancer Drugs To Breast Cancer Cells." *Journal of Molecular Liquids*, 2021.

Gianfaldoni, Serena, Roberto Gianfaldoni, Uwe Wolli, Jacopo Lotti, Georgi Tchernev, and Torello Lotti. "An Overview on Radiotherapy: From Its History to Its Current Applications in Dermatology." *Open Access Macedonian Journal of Medical Sciences*, 2017: 521-525.

Gong, Xing Wen, Dong Zhi Wei, Ming Lei He, and Yu Chun Xiong. "Discarded Free PEG-Based Assay For Obtaining The Modification Extent of Pegylated Proteins ." *Talanta*, 2007: 381-384.

Gong, Zhongying, et al. "pH-Triggered Geometrical Shape Switching of a Cationic Peptide Nanoparticle For Cellular Uptake and Drug Delivery." *Colloids and Surfaces B: Biointerfaces*, 2020.

Harris, Curtis C. "p53 Tumor Suppressor Gene: At the Crossroads of Molecular Carcinogenesis, Molecular Epidemiology and Cancer Risk Assessment." *Environmental Health Perspectives*, 1996: 435-439.

Harvard T.H. Chan School of public health. 2021. https://www.hsph.harvard.edu/nutritionsource/folic-acid/ (erişildi: 10 08, 2021).

Hewlings, Susan J. , and Douglas S. Kalman. "Curcumin: A review of Its' Effect on Human Health." *Foods*, 2017.

Hong, Wei, et al. "pH-Sensitive Micelles For The Intracellular Co-Delivery Of Curcumin and Pluronic L61 Unimers For Synergistic Reversal Effect Of Multidrug Resistance." *Scientific Reports*, 2017: 1-20.

Huang, Kui, Bruce P. Lee, Dale R. Ingram, and Phillip B. Messersmith. "Synthesis and Characterization of Self-Assembling Block Copolymers Containing Bioadhesive End Groups." *Biomacromolecules*, 2002: 397-406.

Jankun , Jerzy, et al. "Determining Whether Curcumin Degradation/Condensation Is Actually Bioactivation (Review)." *International Journal of Molecular Medicine* 37 (2016): 1151-1158.

Jifu, Hao, et al. "Folic Acid-Functionalized Drug Delivery Platform of Resveratrol Based On Pluronic 127/D-α-tocopheryl Polyethylene Glycol 1000 Succinate Mixed Micelles." *International Journal of Nanomedicine*, 2017: 2279-2292.

Laffleur, Flavia , and Valérie Keckeis. "Advances In Drug Delivery Systems: Work In Progress Still Needed?" *International Journal of Pharmaceutics* 590 (2020).

Ledford, Heidi. "The Poisonous History of Chemotherapy." *Nature*, 2020: 346-347.

Liang, Jun F., and Victor C. Yang. "Synthesis of Doxorubicin-Peptide Conjugate with Multidrug Resistant Tumor Cell Killing Activity." *Bioorganic and Medicinal Chemistry Letters*, 08 15, 2005: 5071-5075.

Liu, Mengrui, Hongliang Du, Wenjia Zhang, and Guangxi Zhai. "Internal Stimuli-Responsive Nanocarriers For Drug Delivery: Design Strategies and Applications." *Materials Science and Engineering: C* 71 (2017): 1267-1280.

Lönn, Peter, et al. "Enhancing Endosomal Escape for Intracellular Delivery of Macromolecular Biologic Therapeutics." *Scientific Reports*, 06 08, 2016: 1-9.

Ma, Ziwei , Na Wang, Haibing He, and Xing Tang. "Pharmaceutical Strategies of Improving Oral Systemic Bioavailability of Curcumin For Clinical Application." *Journal of Controlled Release* 316 (2019): 359-380.

Modupe, Oluwasegun, Julie Bloquet Maurras, and Levente L. Diosady. "A Spectrophotometric Method For Determining The Amount of Folic Acid In Fortified Salt." *Journal of Agriculture and Food Research*, 2020.

Mortezaee, Keywan, ve Masoud Najafi. «Immune System in Cancer Radiotherapy: Resistance Mechanisms and Therapy Perspectives.» *Critical Reviews in Oncology/Hematology*, 2020.

Muhamad, Nadda, Tullayakorn Plengsuriyakarn, and Kesara Na-Bangchang. "Application of Active Targeting Nanoparticle Delivery System For Chemotherapeutic Drugs and Traditional/Herbal Medicines In Cancer Therapy: A Systematic Review." *International Journal of Nanomedicine* 13 (2018): 3921-3935.

Patiño-Morales , Carlos César , et al. "Curcumin Stabilizes p53 by Interaction With NAD(P)H:Quinone Oxidoreductase 1 In Tumor-derived Cell Lines." *Redox Biology* 25 (2020).

Pei, Dehua, ve Marina Buyanova. «Overcoming Endosomal Entrapment in Drug Delivery.» *Bioconjugate Chemistry*, 10 12 2018.

Pitto-Barry, Ana¨ıs , and Nicolas P. E. Barry. "Pluronic® Block-Copolymers In Medicine: From Chemical and Biological Versatility To Rationalisation and Clinical Advances." *Royal Society of Chemistry* 5, no. 10 (2014): 3281–3496.

Rapoport, Natalya. "Stabilization and Activation of Pluronic Micelles For Tumor-Targeted Drug Delivery." *Colloids and Surfaces B: Biointerfaces* 16 (1999): 93-111.

Rodrigues, Vanessa Lopes, et al. "A Novel Curcumin Derivative Which Inhibits P-glycoprotein, Arrests Cell Cycle and Induces Apoptosis In Multidrug Resistance Cells." *Bioorganic & Medical Chemistry* 25, no. 2 (2017): 581-596.

Sahu, Abhishek, Naresh Kasoju, Pranab Goswami, and Utpal Bora. "Encapsulation of Curcumin in Pluronic Block Copolymer Micelles for Drug Delivery Applications." *Journal of Biomaterials Applications* 25 (2011): 619-639.

Sivakumar, T., P. Venkatesan, Manavalan R., and K. Valliappan. "Development of a HPLC Method for the Simultaneous Determination of Losartan Potassium and

Atenolol in Tablets." *Indian Journal of Pharmaceutical Sciences*, February 2007.

The Nobel Prize. 2021. https://www.nobelprize.org/prizes/medicine/1908/ehrlich/biographical (accessed 11 26, 2020).

Tohme, Samer , Richard L. Simmons, and Allan Tsung. "Surgery for Cancer: A Trigger for Metastases." *Cancer* 77, no. 7 (2017): 1548-1552.

Vasir, Jasppreet K. , and Vinod Labhasetwar. "Targeted Drug Delivery In Cancer Therapy." *Technology In Cancer Research & Treatment* 4, no. 4 (2005): 363-374.

Wu, Xiaohan, and Suming Li. "Synthesis of Polyactide/Poly(ethylene glycol) Diblock Copolymers With Functional Endgroups ." *Society of Chemical Industry*, 2012: 1014-1021.

Yao, Jianhui, Jingxian Feng, and Jun Chen. "External-Stimuli Responsive Systems For Cancer Theranostic." *Asian Journal of Pharmaceutical Sciences* 11, no. 5 (2016): 585-595.

Zhang , Yun , et al. "Design of a New pH-Activatable Cell-Penetrating Peptide For Drug Delivery Into Tumor Cells." *Chemical Biology & Drug Design*, 2019: 1884-1893.

Zhang, Dong-wei , Min Fu, Si-Hua Gao, and Jun-Li Liu. "Curcumin and Diabetes: A Systematic Review." *Evidence-Based Complementary and Alternative Medicine* 2013 (2013): 1-16.

Zhao, Liyan, et al. "Curcumin Loaded Mixed Micelles Composed of Pluronic P123 and F68:Preparation, Optimization and In Vitro Characterization." *Colloids and Surfaces B: Biointerfaces* 97 (2012): 101-108.